

One-dimensional orbital fluctuations and the exotic magnetic properties of YVO_3

Andrzej M. Oleś

Max-Planck-Institut für Festkörperforschung, Heisenbergstrasse 1, D-70569 Stuttgart, Germany
Marian Smoluchowski Institute of Physics, Jagellonian University, Reymonta 4, PL-30059 Kraków, Poland

Peter Horsch and Giniyat Khaliullin

Max-Planck-Institut für Festkörperforschung, Heisenbergstrasse 1, D-70569 Stuttgart, Germany
(Dated: 21 December 2006)

Starting from the Mott insulator picture for cubic vanadates, we derive and investigate the model of superexchange interactions between V^{3+} ions, with nearly degenerate t_{2g} orbitals occupied by two electrons each. The superexchange interactions are strongly frustrated and demonstrate a strong interrelation between possible types of magnetic and orbital order. We elucidate the prominent role played by fluctuations of yz and xz orbitals which generate ferromagnetic superexchange interactions even in the absence of Hund's exchange. In this limit we find orbital valence bond state which is replaced either by C -type antiferromagnetic order with weak G -type orbital order at increasing Hund's exchange, or instead by G -type antiferromagnetic order when the lattice distortions stabilize C -type orbital order. Both phases are observed in YVO_3 and we argue that a dimerized C -type antiferromagnetic phase with stronger and weaker FM bonds alternating along the c axis may be stabilized by large spin-orbital entropy at finite temperature. This suggests a scenario which explains the origin of the exotic C -AF order observed in YVO_3 in the regime of intermediate temperatures and allows one to specify the necessary ingredients of a more complete future theory.

[Published in: *Phys. Rev. B* **75**, 184434 (2007).]

PACS numbers: 75.10.Jm, 05.70.Fh, 75.30.Et, 75.50.Ee

I. ORBITAL DEGREES OF FREEDOM

Transition metal oxides with the perovskite structure display a large variety of properties such as high-temperature superconductivity and colossal magnetoresistance. Their magnetic properties are also quite diverse, with antiferromagnetic (AF), disordered, or ferromagnetic (FM) phases in different doping regimes, being the subject of particularly active research in the last decade.^{1,2} Although certain universal principles can be formulated, these complex magnetic properties depend on the actual filling of $3d$ orbitals of transition metal ions, and have to be studied in detail for each family of compounds separately. Rich and complex behavior in doped systems is found as moving charges can dress by spin or orbital excitations.³ The undoped compounds are somewhat simpler as their properties are dominated by large on-site Coulomb interactions $\propto U$, responsible for their Mott-Hubbard (or charge-transfer) insulating behavior, with the effective low-energy magnetic interactions of superexchange type. While such interactions are AF and nonfrustrated on a cubic lattice for nondegenerate orbitals, they have a very nontrivial structure when degenerate $3d$ orbitals are partly occupied, as pointed out by Kugel and Khomskii on the example of e_g systems long ago.⁴ In such cases the *orbital degrees of freedom* have to be considered on equal footing with electron spins,^{4,5} which leads to the so-called spin-orbital superexchange models,^{6,7,8,9} describing the low-energy physics and the partial sum rules in the optical spectroscopy.¹⁰

An intriguing feature of the spin-orbital models is the strong frustration of the superexchange interactions on

a cubic (perovskite) lattice which was recognized as the origin of enhanced quantum effects in transition metal oxides.¹¹ For purely electronic models this frustration might even lead to the collapse of long range order in particular parameter regimes, but usually this does not happen and the fluctuations are partly suppressed either by the order-out-of-disorder mechanism,¹² or by the coupling to the lattice distortions induced by the Jahn-Teller (JT) effect. In the cuprates and manganites both the superexchange and the JT interactions support each other,^{13,14} and such systems undergo usually structural transitions. Nevertheless, even below the structural transition the spin and orbital degrees of freedom are coupled, leading to characteristic changes of the orbital order (OO) at magnetic transitions and to new composite spin-orbital excitations, when both spin and orbital excitation occurs simultaneously.¹⁵

The importance of the orbital degrees of freedom was realized in the theory of magnetism already in the seventies. Next to e_g systems,¹⁶ model Hamiltonians with twofold degeneracy and diagonal hopping,¹⁷ and the realistic effective Hamiltonian for t_{2g} electrons in V_2O_3 were studied.¹⁸ Actually, the superexchange interactions for partly filled t_{2g} orbitals are different and even more fascinating than those for e_g systems. As realized first for the d^1 configuration in cubic titanates,¹⁹ the quantum effects are here even stronger than in the e_g systems (cuprates or manganites), as the JT coupling is weak and the orbitals may form the coherent orbital liquid state observed in a Mott insulator LaTiO_3 .²⁰ As a result of this quantum behavior and common spin-orbital fluctuations, the classical Goodenough-Kanamori rules are violated in t_{2g} systems in some cases.²¹

The quantum effects are equally important in vanadium compounds with V^{3+} ions in the d^2 configuration, realized in V_2O_3 and in cubic compounds: $LaVO_3$ and YVO_3 . The metal-insulator transition in V_2O_3 is studied for quite a long time,¹ but more realistic superexchange models were introduced only after the experimental evidence of the OO which occurs below the magnetic transition.²² The first spin-orbital model for V_2O_3 was assuming a picture of molecular bonds which saturated one t_{2g} electron per V^{3+} site and thus used $s = 1/2$ spins.¹⁸ However, one decade ago it was realized that Hund's exchange J_H is large,²³ and the superexchange interactions couple instead $S = 1$ spins of different V^{3+} ions. A complete superexchange model with spin and orbital degrees of freedom in V_2O_3 was derived only a few years ago by Di Matteo, Perkins and Natoli.²⁴

Also in cubic vanadates evidence increases that the orbital degrees of freedom couple to the magnetic order and play an important and highly nontrivial role. In $LaVO_3$ the C -type AF (C -AF) phase [with FM chains along c axis which stagger within ab planes] is stable below Néel temperature $T_N \simeq 143$ K, followed by a weak structural transition at $T_s \simeq 141$ K.^{25,26,27,28,29,30} Remarkably, the magnetic order parameter in the C -AF phase of $LaVO_3$ is strongly reduced to $\simeq 1.3\mu_B$.²⁶ As the spin quantum fluctuations are smaller than in the G -AF phase and are unlikely to decrease the order parameter by more than 6% for $S = 1$ spins,³¹ the observed large reduction of the magnetic moments suggests that some other quantum effects which originate from the orbital degeneracy dominate in this phase of cubic vanadates.

The situation is very different and even more puzzling in YVO_3 ^{29,30,32,33,34,35} — this compound has G -type AF order (staggered in all three directions, called below G -AF) at low temperatures $T < T_{N2}$, while the magnetic order changes in the first order magnetic transition at $T_{N2} = 77$ K to C -AF structure which remains stable up to $T_{N1} \simeq 116$ K. The magnetic transition at T_{N2} is particularly surprising as the staggered moments change their direction from approximately parallel to the c axis in the G -AF phase to lying almost within the ab planes in the C -AF phase, with some small alternating G -AF-like component.³³ In addition, the magnetization is strongly reduced at $T > T_{N2}$, being only close to $1.0\mu_B$ in the C -AF phase,³² and the magnetic exchange constants J_{ab} and $|J_c|$ are there much lower than those found in the low-temperature G -AF phase.³⁶ Even more surprising is the observed gap in the spin wave spectrum which suggests an exotic dimerized structure with alternating stronger and weaker FM exchange constants along c axis.^{36,37} In addition, recent Raman experiments³⁰ suggest that the short-range orbital fluctuations of the orbital G -type occur in this intermediate C -AF phase in addition to the alternating orbital (AO) C -type (C -AO) order, and make it thus quite different from the one observed in $LaVO_3$. We also note that the competition between C -AF and G -AF phase is a common feature of a few vanadate compounds with low atomic radii.³⁰

The electronic structure calculations gave valuable information about the possible charge distribution over the t_{2g} orbitals in YVO_3 .^{38,39} Large on-site Coulomb interaction U prevents double occupancy of d orbitals — it is implemented in the calculations using the local density approximation (LDA) within the so-called LDA+ U method.⁴⁰ The commonly accepted picture is that the xy orbitals are occupied by one electron, while the second one occupies either yz or xz orbital. The lattice distortions in YVO_3 are larger in the low-temperature phase and suggest C -AO order. Above T_{N2} the distortions decrease and are compatible with a weak G -type AO (G -AO) order.³⁴ Theoretical analysis within the charge-transfer model has shown that both phases are indeed energetically close,⁴¹ and one may thus expect that small changes of the thermodynamic potential around T_{N2} could induce a first order phase transition.

In this paper we study the magnetic properties of cubic vanadates with a spin-orbital model derived for vanadates some time ago.⁴² This model applies to Mott insulators with transition metal ions with partly filled t_{2g} orbitals in either d^2 or d^4 configuration. Therefore, this model was recently used to analyze the magnetic structure of monolayer ruthenates.⁴³ In the context of vanadates we have already shown before that the orbital fluctuations play a prominent role in this model and amplify the FM coupling along the c axis, providing a microscopic explanation of the observed C -AF order in $LaVO_3$. In fact, FM interactions induced by Hund's exchange $\propto J_H$ alone are typically much weaker than the AF ones, and would not be sufficient to explain why the FM interactions are *even stronger* than the AF ones in the high temperature C -AF phase of YVO_3 .

Here we will concentrate on the exotic magnetic properties of YVO_3 and address several open questions motivated by the observed magnetic properties, in particular why: (i) the spin exchange interactions are so different in G -type and C -type AF phases of YVO_3 , (ii) the magnetic transition at T_{N2} takes place, (iii) the order parameter $\langle S^z \rangle$ in the C -AF is so strongly reduced, and finally, (iv) the dimerization along the c axis, observed in the C -AF phase in the intermediate regime of temperature $T_{N2} < T < T_{N1}$, takes place. A careful discussion of these questions in the context of the microscopic model will lead us to a scenario for the exotic magnetic properties of the intermediate temperature phase of YVO_3 consistently explained within a *dimerized* C -AF order stable only at finite temperature, and characterized by reduced exchange interactions. At the same time, we will argue that further theoretical studies are necessary in order to explain all the observed properties.

The paper is organized as follows. In Sec. II we present the spin-orbital model for cubic vanadates. It is derived from the degenerate Hubbard model (Sec. II A) and contains superexchange interactions supplemented by orbital interactions induced by the lattice (Sec. II B). Next we introduce the possible types of classical order in Sec. III, emphasizing first the tendency towards one-dimensional

(1D) orbital fluctuations (Sec. III A), and next comparing their classical energies (Sec. III B). The effective exchange interactions in different magnetic phases are evaluated in Sec. IV A. For the magnetic phases stable in different regimes of parameters we derive spin (Sec. IV B) and orbital (Sec. IV C) excitations, which serve next to calculate the quantum corrections to the energy and lead to the phase diagram of the model at $T = 0$ of Sec. IV D.

Using the above background information we propose a scenario for the magnetic phase transition at T_{N2} in YVO_3 in Sec. V. The unique instability of the 1D spin-orbital chain (Sec. V A) comes here together with the reduction of the magnetic exchange constants by orbital fluctuations (Sec. V B) to stabilize the dimerized C -AF phase at temperature $T > T_{N2}$, as we show by analyzing the spin and orbital entropy contributions to the free energy (Sec. V C). In Sec. VI we summarize the results and present general conclusions. The paper includes two appendices which present the derivation of the spin-orbital model for cubic vanadates (Appendix A), and the calculation of spin and orbital excitations, as well as the average order parameters, and intersite (spin and orbital) correlations at finite temperature in the dimerized C -AF phase (Appendix B).

II. SPIN-ORBITAL MODEL FOR CUBIC VANADATES

A. Degenerate Hubbard model for t_{2g} electrons

We consider a realistic degenerate Hubbard model for $3d$ electrons of V^{3+} ions in cubic vanadates, with partly filled t_{2g} orbitals that are energetically favored over e_g orbitals by the octahedral field. Thereby, we neglect small lattice distortions and the tilting of VO_6 octahedra. Therefore, the e_g orbitals do not couple to t_{2g} orbitals by the hopping processes and play no role in the magnetic properties we address below. In such an (idealized) perovskite structure V^{3+} ions occupy the cubic lattice, and the hopping elements between active t_{2g} orbitals are the same in all three cubic directions. The model Hamiltonian,

$$\mathcal{H} = H_t + H_{\text{cf}} + H_{\text{int}}, \quad (2.1)$$

includes the kinetic energy H_t , the orbital splittings induced by the crystal field H_{cf} , and the on-site electron-electron interactions H_{int} . The kinetic energy is described by the effective hopping element t between two V^{3+} ions which originates from two hopping processes via the $2p_\pi$ oxygen orbital along each Mn–O–Mn bond. Its value can in principle be derived from the charge-transfer model,^{3,23} and one expects $t = t_{pd}^2/\Delta \sim 0.2$ eV. A more accurate estimation from the theory is not possible at the moment, so we will have to rely on experimental information from neutron scattering concerning the magnetic exchange constants in YVO_3 .

The kinetic energy is given by:

$$H_t = -t \sum_{\langle ij \rangle \parallel \gamma} \sum_{\mu(\gamma), \sigma} \left(d_{i\mu\sigma}^\dagger d_{j\mu\sigma} + d_{j\mu\sigma}^\dagger d_{i\mu\sigma} \right), \quad (2.2)$$

where $d_{i\nu\sigma}^\dagger$ are electron creation operators, and the summation runs over the bonds $\langle ij \rangle \parallel \gamma$ along three cubic axes, $\gamma = a, b, c$. As observed before,^{19,42} only two out of three t_{2g} orbitals, labelled by $\mu(\gamma)$, are active along each bond $\langle ij \rangle$ and contribute to the kinetic energy (2.2), while the third orbital lies in the plane perpendicular to the γ axis and the hopping via the $2p_\pi$ oxygen is forbidden by symmetry. This motivates a convenient notation used below,

$$|a\rangle \equiv |yz\rangle, \quad |b\rangle \equiv |xz\rangle, \quad |c\rangle \equiv |xy\rangle, \quad (2.3)$$

with the inactive orbital along a given cubic direction γ , labelled by its index as $|\gamma\rangle$.

The electron-electron interactions are described by the on-site terms,⁴⁴

$$\begin{aligned} H_{\text{int}} = & U \sum_{i\mu} n_{i\mu\uparrow} n_{i\mu\downarrow} + \left(U - \frac{5}{2} J_H \right) \sum_{i, \mu < \nu, \sigma\sigma'} n_{i\mu\sigma} n_{i\nu\sigma'} \\ & - 2J_H \sum_{i, \mu < \nu} \vec{S}_{i\mu} \cdot \vec{S}_{i\nu} + J_H \sum_{i, \mu \neq \nu} d_{i\mu\uparrow}^\dagger d_{i\mu\downarrow}^\dagger d_{i\nu\downarrow} d_{i\nu\uparrow}, \end{aligned} \quad (2.4)$$

with U and J_H standing for the intraorbital Coulomb and on-site Hund's exchange interaction, respectively, using the notation of Kanamori.⁴⁵ Each pair of orbitals $\{\mu, \nu\}$ is included only once in the respective interaction terms with summations over $\mu < \nu$. The Hamiltonian (2.4) describes rigorously the multiplet structure of d^2 and d^3 ions within the t_{2g} subspace⁴⁶ and is rotationally invariant in the orbital space.⁴⁴ More precisely, the on-site Coulomb interactions depend on three Racah parameters $\{A, B, C\}$, and for t_{2g} orbitals one finds,

$$U = A + 4B + 3C, \quad J_H = 3B + C, \quad (2.5)$$

The Coulomb and exchange element, U and J_H , can be thus obtained using the spectroscopic information about the Racah parameters for V^{2+} ions in the excited states: $A = 3.54$ eV, $B = 0.095$ eV, and $C = 0.354$ eV, as given by Zaanen and Sawatzky.⁴⁷ With these parameters one finds $U = 5.0$ eV and $J_H = 0.64$ eV.

The Coulomb element U is therefore sufficiently large compared to $t \sim 0.2$ eV (i.e., $U \gg t$) to use the second order perturbation theory in which the charge fluctuations $d_i^2 d_j^2 \equiv d_i^3 d_j^1$ are suppressed, and the d electrons are localized in t_{2g}^2 configurations of a Mott insulator (The interaction parameters for V^{3+} ions have similar values to those of V^{2+} ones). We use this picture as a starting point for our analysis and assume that two electrons are localized at each V^{3+} ion i , satisfying a local constraint (at site i) for the total electron density,

$$n_i = n_{ia} + n_{ib} + n_{ic} = 2, \quad (2.6)$$

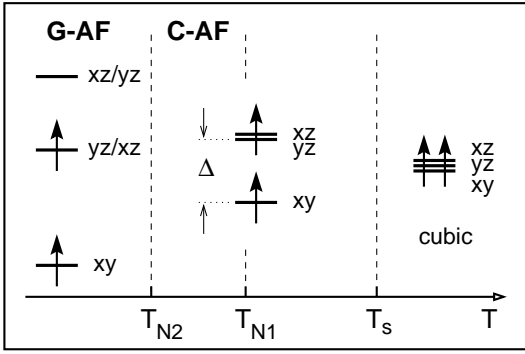


FIG. 1: An artist view of the energy splittings between t_{2g} orbitals in YVO_3 in different temperature regimes. The orbital splitting Δ which occurs below the structural transition at T_s and persists in the C -AF phase favors the occupied xy orbitals, but allows also for weak orbital fluctuations. Such fluctuations are quenched in the G -AF phase at $T < T_{N2}$.

where $n_{ia} = \sum_{\sigma} n_{ia\sigma}$, etcetera. Two electrons at every site are in the high-spin 3T_2 triplet ($S = 1$) state, stabilized by Hund's exchange J_H . As $t \ll J_H$, the kinetic energy H_t can only contribute in virtual processes which are responsible for the superexchange interactions derived below in Sec. II B.

The third term in Eq. (2.1) stands for the orbital energies in crystal field induced by the structural transition at $T_s \sim 200\text{K}$,³⁴ which lifts the degeneracy of three t_{2g} orbitals and breaks the cubic symmetry in the orbital space. We write the crystal field term H_{cf} as follows,

$$H_{cf} = \sum_{i\mu} \varepsilon_{i\mu} n_{i\mu}, \quad (2.7)$$

with electron energies $\varepsilon_{i\mu}$ for orbital μ at site i . In agreement with the results of band structure calculations,^{38,39} and with an idealized but suggested by the local distortions and thus commonly accepted picture,³³ we assume that the xy orbitals are favored below the structural transition, while the remaining yz and xz orbitals are nearly degenerate, i.e., $\varepsilon_c < \varepsilon_a$, and $\varepsilon_b \simeq \varepsilon_a$, leading to

$$n_{ic} \simeq 1, \quad n_{ia} + n_{ib} \simeq 1, \quad (2.8)$$

i.e., c orbitals are 'condensed' and the other two represent the remaining t_{2g} orbital degree of freedom at every site (see Fig. 1). Although in principle the orbital energies $\varepsilon_{i\mu}$ could change at the magnetic transition at T_{N2} and further stabilize G -AF phase at low temperature, we will ignore small corrections which would result from this effect in the derivation of the superexchange, and consider only generic features of the spin-orbital model that could be responsible for the experimental situation.

B. Superexchange model for vanadates

Consider first the atomic limit, i.e., the system of V^{3+} ions in d^2 configuration at $t = 0$. In the ground state

$S = 1$ spin forms at each ion, and one finds a large degeneracy 9^N of the ground state, where N is the number of sites, as every spin component ($S^z = 1, 0, -1$) is allowed, and a hole may occupy either orbital: $|a\rangle$, $|b\rangle$ or $|c\rangle$. This large degeneracy is, however, removed by the effective interactions between each pair of nearest neighbor ions $\{i, j\}$, which originate from virtual transitions to the excited states due to charge $d_i^2 d_j^2 \Rightarrow d_i^3 d_j^1$ excitations, generated in each case by a single hopping of a t_{2g} electron. In the realistic regime of parameters such processes may be treated perturbatively, and one arrives in second order perturbation theory at an effective superexchange Hamiltonian of Ref. 42 — the details of the derivation are explained in Appendix A.

The superexchange interactions between two $S = 1$ spins at sites i and j arise from virtual excitations $d_i^2 d_j^2 \rightarrow d_i^3 d_j^1$ along the concerned bond $\langle ij \rangle$, promoted by the hopping t which couples pairs of identical *active* t_{2g} orbitals. A single hopping process generates a d_i^3 configuration, either with three different orbitals occupied by a single electron each, or with a double occupancy in one of the two active orbitals (see Fig. 2). Therefore, the d_i^3 excited state may be either a high-spin 4A_2 state, or one of three low-spin states: 2E , 2T_1 or 2T_2 with energies⁴⁸ $U - 3J_H$, U and $U + 2J_H$, as shown in Fig. 1 of Ref. 9. This perturbative consideration leads to the spin-orbital superexchange model for cubic vanadates,

$$\mathcal{H}_J = J \sum_{\langle ij \rangle \parallel \gamma} \left[(\vec{S}_i \cdot \vec{S}_j + 1) \hat{J}_{ij}^{(\gamma)} + \hat{K}_{ij}^{(\gamma)} \right]. \quad (2.9)$$

with the energy scale given by the superexchange constant,

$$J = \frac{4t^2}{U}. \quad (2.10)$$

The spin interactions $\propto \vec{S}_i \cdot \vec{S}_j$ obey the $SU(2)$ symmetry. In contrast, the orbital interaction operators $\hat{J}_{ij}^{(\gamma)}$ and $\hat{K}_{ij}^{(\gamma)}$ involve only two active t_{2g} orbitals on each individual bond $\langle ij \rangle \parallel \gamma$ ($\gamma = a, b, c$) which contribute to the virtual excitations, so they have a lower (cubic) symmetry. These operators take the form:

$$\begin{aligned} \hat{J}_{ij}^{(\gamma)} &= \frac{1}{2} \left[(1 + 2\eta r_1) \left(\vec{\tau}_i \cdot \vec{\tau}_j + \frac{1}{4} n_i n_j \right) \right. \\ &\quad \left. - \eta r_3 \left(\vec{\tau}_i \otimes \vec{\tau}_j + \frac{1}{4} n_i n_j \right) - \frac{1}{2} \eta r_1 (n_i + n_j) \right]^{(\gamma)} \end{aligned} \quad (2.11)$$

$$\begin{aligned} \hat{K}_{ij}^{(\gamma)} &= \left[\eta r_1 \left(\vec{\tau}_i \cdot \vec{\tau}_j + \frac{1}{4} n_i n_j \right) + \eta r_3 \left(\vec{\tau}_i \otimes \vec{\tau}_j + \frac{1}{4} n_i n_j \right) \right. \\ &\quad \left. - \frac{1}{4} (1 + \eta r_1) (n_i + n_j) \right]^{(\gamma)}, \end{aligned} \quad (2.12)$$

and have a rich structure which originates from the projections of the d_i^3 excited states on the respective eigenstates of V^{2+} ion, as explained in Appendix A.

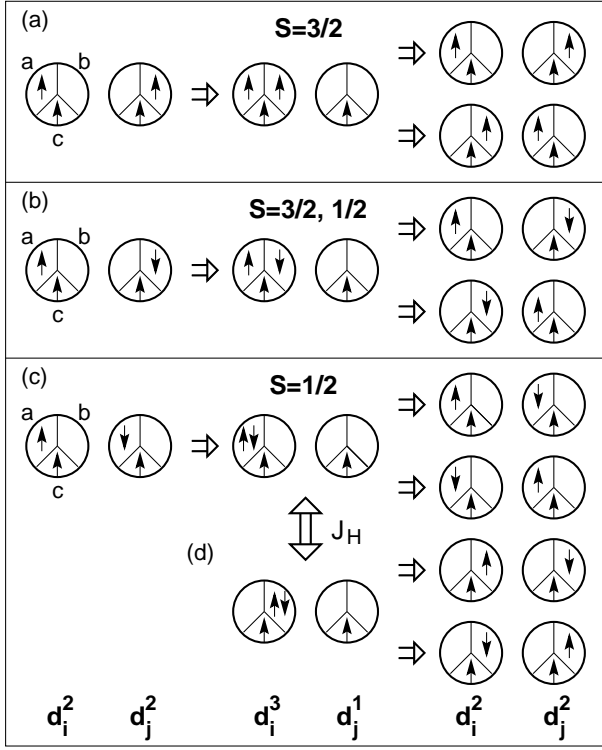


FIG. 2: Virtual charge excitations $d_i^2 d_j^2 \rightarrow d_i^3 d_j^1 \rightarrow d_i^2 d_j^2$ within a bond $\langle ij \rangle$ along c axis, which contribute to the superexchange in cubic vanadates. Orbital fluctuations which support the FM superexchange occur when different active orbitals a and b are occupied at both sites, as in cases (a) and (b). If the same orbitals are occupied at both sites, e.g. the orbital a as in case (c), the superexchange is AF — then a double occupancy of the occupied (and active) orbital is generated in the excited state, which next dissociates to a configuration with either: (c) the same orbital occupancies, or (d) with interchanged occupied orbitals at sites i and j .

First of all, the interactions $\hat{J}_{ij}^{(\gamma)}$ and $\hat{K}_{ij}^{(\gamma)}$ depend on Hund's exchange splittings in the multiplet structure of a V^{2+} ion in local d^3 configuration (shown in Fig. 1 of Ref. 9) via the exchange parameter,

$$\eta = \frac{J_H}{U}, \quad (2.13)$$

and the respective coefficients r_1 and r_3 in Eqs. (2.11) and (2.12) are (for convenience we use here the same notation as in Ref. 9):

$$r_1 = \frac{1}{1-3\eta}, \quad r_3 = \frac{1}{1+2\eta}. \quad (2.14)$$

They correspond to the excitation spectrum in $d_i^2 d_j^2 \rightleftharpoons d_i^3 d_j^1$ charge transitions (Fig. 2). In the present case of cubic vanadates one finds⁴⁷ $\eta \simeq 0.13$, which we will take as a representative value for YVO_3 .

The pseudospin (orbital) operators $\vec{\tau}_i = \{\tau_i^+, \tau_i^-, \tau_i^z\}$ for pseudospin $\tau = 1/2$ in Eqs. (2.11) and (2.12) are defined in the subspace spanned by two orbital flavors

which are active along a given direction γ . For instance, the virtual transitions which generate the superexchange interactions follow from the electron hopping between the pairs of active a and b orbitals along the bond $\langle ij \rangle \parallel c$ axis (see Fig. 2), and these operators are defined by Eqs. (A6), while the number of active electrons at site i is $n_i^{(c)} = n_{ia} + n_{ib}$. It is important to realize that although the pseudospin flavor is conserved in each individual hopping processes, the off-diagonal elements of the Coulomb interaction $\propto J_H$ generate transitions between the components of the excited states, as shown in Fig. 2(d).⁴⁹ Therefore, next to the usual scalar products,

$$2 \left(\vec{\tau}_i \cdot \vec{\tau}_j + \frac{1}{4} n_i n_j \right)^{(c)} \equiv (n_{ia} n_{ja} + a_i^\dagger b_i b_j^\dagger a_j) + (a \leftrightarrow b), \quad (2.15)$$

we also find in the orbital operators $\hat{J}_{ij}^{(\gamma)}$ and $\hat{K}_{ij}^{(\gamma)}$ 'orbital fluctuating' terms

$$2 \left(\vec{\tau}_i \otimes \vec{\tau}_j + \frac{1}{4} n_i n_j \right)^{(c)} \equiv (n_{ia} n_{ja} + a_i^\dagger b_i a_j^\dagger b_j) + (a \leftrightarrow b), \quad (2.16)$$

where $(a \leftrightarrow b)$ stands for the terms with interchanged a and b orbitals. Unlike in the Heisenberg model, the interactions $\propto \tau_i^+ \tau_j^+ = a_i^\dagger b_i a_j^\dagger b_j$ in Eq. (2.16) induce *similar* orbital flips at both sites. Such terms have the form

$$(\vec{\tau}_i \otimes \vec{\tau}_j)^{(c)} = \frac{1}{2} (\tau_i^+ \tau_j^+ + \tau_i^- \tau_j^-) + \tau_i^z \tau_j^z \quad (2.17)$$

and lead to the nonconservation of the total pseudospin quantum number and are thus responsible for further enhancement of orbital quantum fluctuations on the bonds with both orbitals active (in this case along c axis). In contrast, the bonds in ab planes are classical as there analogous terms cannot contribute when the c orbitals have condensed. This demonstrates that the breaking of symmetry in the orbital space, such as given by Eqs. (2.8), will have severe consequences for magnetism.

The complete microscopic model we consider in the following Sections,

$$\mathcal{H} = \mathcal{H}_J + \mathcal{H}_{\text{orb}}, \quad (2.18)$$

includes as well effective orbital interactions induced by the oxygen distortions. When the VO_6 octahedra distort at a second magnetic transition at T_{N2} ,^{32,35} intersite interactions which help to order yz and xz orbitals, occupied by one electron at every site, are induced. They are of two types — the $GdFeO_3$ -type distortions favor repeated orbitals along the c axis, while the AO order in ab planes is favored by weak JT effect. Therefore, in addition to the superexchange (2.9) we introduce two effective orbital interactions $\{V_c, V_a\}$ as the last term of the effective Hamiltonian (2.18),

$$\mathcal{H}_{\text{orb}} = -V_c \sum_{\langle ij \rangle \parallel c} \tau_i^z \tau_j^z + V_a \sum_{\langle ij \rangle \parallel ab} \tau_i^z \tau_j^z, \quad (2.19)$$

where the orbital pseudospin operator τ_i^z at site i is defined by Eq. (A7). With the present sign convention both parameters are positive ($V_c > 0$ and $V_a > 0$) and induce the C -type AO (C -AO) order, as observed in the G -AF phase at $T < T_{N_2}$. For convenience we express the orbital interactions in \mathcal{H}_{orb} (2.19) in the units of the superexchange constant J , and introduce dimensionless parameters:

$$v_a = \frac{V_a}{J} \quad v_c = \frac{V_c}{J}, \quad (2.20)$$

which describe the model given by Eq. (2.18), in addition to Hund's exchange parameter η .

III. TYPES OF MAGNETIC ORDER

A. Orbital singlets at $J_H \rightarrow 0$

In order to understand the possible symmetry breaking in the cubic vanadates, consider first the superexchange interactions in the $J_H \rightarrow 0$ limit:

$$\mathcal{H}_0 = \frac{1}{2}J \sum_{\langle ij \rangle \parallel \gamma} \left(\vec{S}_i \cdot \vec{S}_j + 1 \right) \left(\vec{\tau}_i \cdot \vec{\tau}_j + \frac{1}{4}n_i n_j \right)^{(\gamma)}, \quad (3.1)$$

where a constant energy of $-2J$ per V^{3+} ion is neglected. It is straightforward to understand why the interactions at $J_H \rightarrow 0$ turn out to have the same structure as in LaTiO_3 ,¹⁹ where for spins $s = 1/2$ of Ti^{3+} ions one finds instead the spin part $4(\vec{s}_i \cdot \vec{s}_j + \frac{1}{4})$. In fact, in the limit of $J_H \rightarrow 0$ the superexchange interactions follow entirely from the *Pauli principle*, as the multiplet structure of excited states collapses to a single degenerate level and the spin interactions $\propto \vec{S}_i \cdot \vec{S}_j$ due to the high-spin 4A_2 and low-spin 2E states, which involve $d^3\{abc\}$ configurations, cancel each other (see Appendix A). This suggests that the superexchange interactions might *all* be AF in the limit of $J_H \rightarrow 0$, as in e_g systems.^{7,11} In fact, in e_g systems only one directional orbital is active along the bond, two electrons occupying these orbitals form an *intraorbital spin singlet*, which maximizes the energy gain for the AF superexchange.

However, there is an important difference between the e_g (with one hole per site) and t_{2g} (with one or two electrons per site) systems, which may be best realized by considering a single bond $\langle ij \rangle$ in one cubic direction. Two active t_{2g} orbitals along this bond open a new possibility — if both orbitals are singly occupied, an *orbital singlet* gives here FM superexchange, even in the absence of Hund's exchange J_H .⁴² For the present filling of $n = 2$ electrons per site, and if $n_c = 1$, such a resonance on a bond is possible only along one out of three cubic directions⁵⁰ — the orbital singlets and uncorrelated bonds alternate along the c axis [Fig. 3(a)]. In analogy with spin systems,⁵¹ this state can be called an *orbital valence bond* (OVB) state.⁵² This possibility was also independently pointed out by Shen, Xie and Zhang,⁵³ who

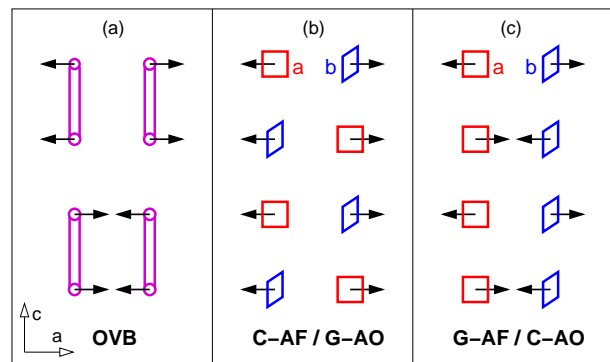


FIG. 3: (Color online) Schematic picture of the classical phases with magnetic and orbital order for $n_{ic} = 1$ in ac plane: (a) OVB phase, with alternating strong FM bonds stabilized by orbital singlets represented by double lines, and weak AF bonds (with disordered a/b orbitals); (b) C -AF spin order accompanied by G -AO order; and (c) G -AF spin order accompanied by C -AO order with repeated either a or b orbitals along c axis. In cases (b) and (c) spins and orbitals alternate along b direction (not shown). These latter states follow the Goodenough-Kanamori rules^{5,54} and are analyzed below for YVO_3 .

obtained the OVB state as the most stable solution of the present Hamiltonian (2.9) in the regime of small η and for large S limit.

The OVB state implies an unconventional type of magnetic order. At $\eta = 0$ the exchange constants along the c axis are given by

$$J_c(\eta = 0) = \left\langle \vec{\tau}_i \cdot \vec{\tau}_j + \frac{1}{4}n_i n_j \right\rangle^{(c)}. \quad (3.2)$$

When the orbital singlets form and contribute to the energy with $\langle \vec{\tau}_i \cdot \vec{\tau}_j \rangle^{(c)} = -\frac{3}{4}$, they maximize the FM exchange on these bonds [see Sec. IV A], and stabilize there effective $S = 2$ spin states. Between them one finds disordered orbitals, i.e., $\langle \vec{\tau}_i \cdot \vec{\tau}_j \rangle^{(c)} = 0$, so the magnetic exchange interactions on these bonds are much weaker and are in fact AF due to the static term $\langle n_i n_j \rangle^{(c)} = 1$ in Eq. (3.2). The interactions within the ab planes are also AF but somewhat stronger — they follow from the conventional (Pauli principle) mechanism which operates as well in the absence of orbital degeneracy, with *intraorbital* singlets generated by the nearest neighbor hopping between sites with singly occupied c orbitals (2.8). Assuming disordered orbitals one finds $\langle \vec{\tau}_i \cdot \vec{\tau}_j \rangle^{(ab)} = 0$ and $\langle n_i n_j \rangle^{(ab)} = \frac{5}{2}$ for the bonds in ab planes. The resulting magnetic order which coexists with the orbital singlets is shown in Fig. 3(a).

B. Magnetic and orbital order at finite J_H

Let us analyze the possible types of coexisting magnetic and orbital order of the full effective Hamiltonian given by Eq. (2.18) for finite Hund's exchange J_H , which

includes the effective orbital interactions $\{V_a, V_c\}$ with the lattice. Motivated by the experimental situation in YVO_3 , we assume that the c orbitals have condensed, so the constraints given by Eqs. (2.8) are fulfilled. For this case we consider possible classical phases and their energies. A more complete analysis which includes the quantum corrections due to spin and orbital excitations is presented in Sec. IV D, here we discuss only a qualitative picture when spin quantum fluctuations are neglected.

At $\eta = 0$ the lowest energy is obtained when the orbital fluctuations are fully developed at every second bond along the c axis in the OVB state,^{36,37,53} as discussed in Sec. III A. The classical energy of this phase per site is obtained assuming the classical values for intersite spin correlations: $\langle \vec{S}_i \cdot \vec{S}_j \rangle = \pm 1$ on the FM/AF bonds. It includes the orbital fluctuation energy gained on the orbital singlet bonds and is given by:

$$E_{\text{OVB}}^{(0)} = -J \left[\frac{1}{4}r_1 + \frac{1}{8}\eta(9r_1 - 11r_3) - \frac{1}{8}v_c \right]. \quad (3.3)$$

Here and below we neglect a constant nonmagnetic term $-2J$. Except for the orbital singlets, the orbital interactions in \mathcal{H}_{orb} do not contribute as the $\{a, b\}$ orbitals are disordered on all other bonds [Fig. 3(a)].

An alternative AF state, realized at larger values of η ,⁴² is obtained when the (negative) orbital correlations along the c axis are uniform, and all the bonds exhibit FM exchange. As the spin interactions remain AF in ab planes, these interactions lead to the C -AF phase shown schematically in Fig. 3(b). A straightforward estimate of the classical energy of this phase,

$$E_C^{(0)} = J \left[r_1 \left\langle \vec{\tau}_i \cdot \vec{\tau}_j + \frac{1}{4} \right\rangle^{(c)} + \eta(r_1 + r_3) \langle n_{ia} n_{ja} \rangle^{(b)} - \eta(2r_1 - r_3) - v_c + 2v_a \right], \quad (3.4)$$

is obtained again taking the classical spin correlations: $\langle \vec{S}_i \cdot \vec{S}_j \rangle^{(c)} = 1$ and $\langle \vec{S}_i \cdot \vec{S}_j \rangle^{(ab)} = -1$. It depends on the orbital correlations $\langle \vec{\tau}_i \cdot \vec{\tau}_j \rangle$. Taking fully disordered 1D orbital chain with $\langle \vec{\tau}_i \cdot \vec{\tau}_j \rangle = -0.4431$, as for the AF Heisenberg spin chain,⁵⁵ one finds a crossover from the OVB to the C -AF phase at $\eta_0 \simeq 0.064$. We improve this naive estimate of the transition in Sec. IV D, where we evaluate the quantum corrections due to spin excitations in both phases.

Unlike in e_g systems,^{13,14} the orbital interactions induced by the lattice (2.19) compete with the superexchange (2.9) in the present effective spin-orbital model (2.18) and stabilize the G -AF phase at sufficiently large orbital interaction V_c .⁴² The classical energy of this phase,

$$E_G^{(0)} = -J \left[\eta(r_1 - r_3) + \frac{1}{4}v_c + \frac{1}{2}v_a \right], \quad (3.5)$$

is lowered by the energy $-\frac{1}{4}J(v_c + 2v_a)$ gained per site when the C -AO order shown in Fig. 3(c) sets in. In fact,

the C -AO order enforces here the G -AF phase, showing a close interrelation of spin and orbital intersite correlations, known in the literature as the Goodenough-Kanamori rules.^{5,54}

IV. SPIN AND ORBITAL EXCITATIONS

A. Effective exchange interactions

In order to analyze the spin and orbital excitations, we follow the usual approach in mean field theory⁹ and decouple spin and orbital operators in Eq. (2.9). Note that this approach is satisfactory below the spin ordering temperature T_{N1} , as then the spin fluctuations are quenched and the spin and orbital degrees of freedom may be disentangled,²¹ while for $T > T_{N1}$ composite spin-orbital excitations need to be considered. This procedure leads to the effective spin exchange constants J_c and J_{ab} , as given in Refs. 9,10,

$$J_c = -\frac{1}{2}J \left[\eta r_1 - (r_1 - \eta r_1 - \eta r_3) \times \left\langle \vec{\tau}_i \cdot \vec{\tau}_j + \frac{1}{4} \right\rangle^{(c)} - 2\eta r_3 \left\langle \tau_i^y \tau_j^y \right\rangle^{(c)} \right], \quad (4.1)$$

$$J_{ab} = \frac{1}{4}J \left[1 - \eta r_1 - \eta r_3 + (r_1 - \eta r_1 - \eta r_3) \left\langle \tau_i^z \tau_j^z + \frac{1}{4} \right\rangle^{(a)} \right]. \quad (4.2)$$

They depend on the orbital correlations, $\langle \vec{\tau}_i \cdot \vec{\tau}_j \rangle$ and $\langle \tau_i^y \tau_j^y \rangle$ along c axis, and $\langle \tau_i^z \tau_j^z \rangle$ in ab planes, which have to be determined from the full superexchange model given by Eq. (2.18), i.e., in presence of orbital interactions promoted by the lattice. Below we specify the effective exchange interactions for three possible phases shown in Fig. 3.

At low η one expects that the OVB state with alternating FM and AF bonds along c axis is stable [Fig. 3(a)]. On the bonds occupied by orbital singlets, with $\langle \vec{\tau}_i \cdot \vec{\tau}_j \rangle^{(c)} = -\frac{3}{4}$ and $\langle \tau_i^y \tau_j^y \rangle^{(c)} = -\frac{1}{4}$, one finds strong FM exchange

$$J_{c1}^O = -\frac{1}{4}J r_1 (1 + \eta), \quad (4.3)$$

which is further enhanced with increasing η and soon becomes the dominating magnetic interaction, see Fig. 4(a). In contrast, for the bonds connecting singlets the orbitals are disordered, $\langle \vec{\tau}_i \cdot \vec{\tau}_j \rangle = \langle \tau_i^y \tau_j^y \rangle = 0$, and the resulting AF exchange interactions

$$J_{c2}^O = \frac{1}{8}J [1 - \eta(2r_1 + r_3)], \quad (4.4)$$

decrease with increasing η . These exchange interactions are much weaker than the AF ones in the ab planes,

$$J_{ab}^O = \frac{5}{16}J [1 - \eta(r_1 + r_3)], \quad (4.5)$$

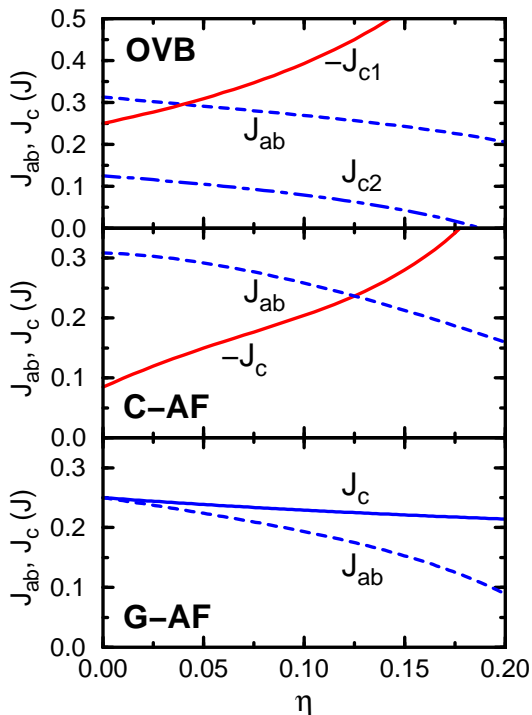


FIG. 4: (Color online) Exchange interactions J_c and J_{ab} as functions of Hund's exchange η as obtained for: (a) OVB phase with alternating strong FM J_{c1} (solid line) and weak AF J_{c2} (dashed-dotted line) exchange interaction; (b) C -AF phase with (weak) G -type OO; and (c) G -AF phase stabilized by the orbital interactions $\{V_a, V_c\}$ which induce the C -AO order. FM (AF) exchange interactions along c axis in C -AF (G -AF) phase are shown by solid lines, while AF interactions in ab planes are shown by dashed lines.

in the entire allowed regime of η , as the latter interactions are supported by the excitations of doubly occupied configurations in c orbitals. One finds that the OVB state with alternating FM and AF bonds is destroyed at a critical value of η ,

$$\eta_0 = \frac{1}{2r_1 + r_3} \simeq 0.188, \quad (4.6)$$

where the weaker AF bond J_{c2} collapses and changes its sign, see Fig. 4(a). In reality, it turns out that the orbital singlets are destabilized even much faster as a better energy is obtained when the spins reorient to FM order and the C -AF phase with uniform disordered (or weakly ordered) $\{a, b\}$ orbitals along the c axis takes over, as we show below.

The simplest possible approach to the C -AF phase is to assume that the coupling to the lattice dominates and stabilizes the G -AO order, as shown in Fig. 3(b). Such a robust OO would lead to classical values of orbital correlations in G -type phases, with $\langle \vec{\tau}_i \cdot \vec{\tau}_j + \frac{1}{4} \rangle^{(c)} = 0$, and $\langle \tau_i^y \tau_j^y \rangle^{(c)} = 0$. However, it was recently pointed out⁹ that this situation does not occur in LaVO_3 , and instead one has to consider fluctuating orbitals. The exchange

constants in the C -AF phase, J_c^C and J_{ab}^C , can be found from the orbital excitations in the 1D disordered orbital chain, and we provide analytic expressions to evaluate them in Sec. IV C. They allow one to determine the (weak) OO parameter $\langle \tau^z \rangle$ and the intersite orbital correlations which appear in Eqs. (4.1) and (4.2). Here we present the result of the numerical calculation, see Fig. 4(b). The FM exchange J_c^C is *finite* already at $\eta = 0$ due to the a/b orbital fluctuations,⁴² and is further enhanced by increasing splitting between the high-spin and low-spin excitations when Hund's exchange η increases. At the same time, the AF exchange interaction J_{ab}^C in ab planes decreases.

Finally, we consider G -AF phase realized in YVO_3 at low temperature $T < T_{N2}$. A classical state with robust C -AO order has been proposed for this phase,³⁴ as shown in Fig. 3(c). We have verified that the quantum corrections to the OO parameter $\langle \tau^z \rangle$ are indeed negligible by considering the orbital waves for such a classical C -AO phase, see Sec. IV C, so one finds indeed rather simple expressions for the AF exchange constants along the c axis and in ab planes:

$$J_c^G = \frac{1}{4}J(1 - \eta r_3), \quad (4.7)$$

$$J_{ab}^G = \frac{1}{4}J[1 - \eta(r_1 + r_3)]. \quad (4.8)$$

Both above coupling constants decrease with increasing Hund's exchange, and the anisotropy between J_c and J_{ab} is gradually enhanced (Fig. 4).

B. Spin wave excitations

The spin waves in different phases can be derived using the linear spin wave (LSW) theory.^{55,56} In the present case of $S = 1$ spins this approach gives reliable results also for the OVB phase, in contrast to the linear orbital wave (LOW) theory for $\tau = 1/2$ pseudospins which cannot be applied to the OVB phase as the a and b orbitals are there disordered. For the AF phases with two (or four) sublattices and the classical AF order $\langle S_i^z \rangle = \pm S$ considered here, we first rotate the spin operators on the sites occupied by down spins (with $\langle S_i^z \rangle = -S$) by angle π with respect to spin x axis, which leads to the canonical transformation:

$$S_i^\pm \Rightarrow -S_i^\pm, \quad S_i^z \Rightarrow -S_i^z. \quad (4.9)$$

Next we write the equations of motion for the spin operators and apply standard Holstein-Primakoff transformation⁵⁵ from spin operators to boson operators (here $S = 1$),

$$S_i^+ \simeq \sqrt{2S}a_i, \quad S_i^- \simeq \sqrt{2S}a_i^\dagger, \quad S_i^z = S - a_i^\dagger a_i. \quad (4.10)$$

The respective boson problem is easily diagonalized by employing first the Fourier transformation and next a Bogoliubov transformation in the momentum space \mathbf{k} .

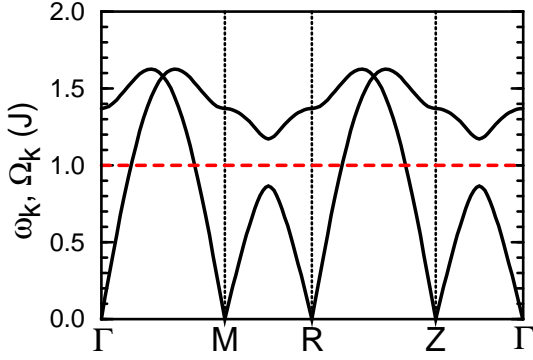


FIG. 5: (Color online) Spin-wave dispersion $\omega_{\mathbf{k}}$ (full lines) and orbital triplet excitation energy $\Omega_{\mathbf{k}}$ (dashed line), as obtained for the OVB phase along high symmetry directions in the Brillouin zone at $\eta = 0$ and $V_c = 0$. For the present parameters one finds the following values of spin exchange constants: $J_{ab} = 0.3125J$, $J_{c1} = -0.250J$ and $J_{c2} = 0.125J$. The high symmetry points are: $\Gamma = (0, 0, 0)$, $M = (\pi, \pi, 0)$, $R = (\pi, \pi, \pi)$, $Z = (0, 0, \pi)$.

Following the above procedure, one finds the spin-wave dispersion in the OVB phase,

$$\omega_{O\pm}(\mathbf{k}) = \left\{ [4J_{ab} + |J_{c1}| + J_{c2}]^2 - [4J_{ab}\gamma(\mathbf{k}) \pm \{(|J_{c1}| + J_{c2})^2 - 4J_{c1}J_{c2}\cos^2 k_z\}^{1/2}] \right\}^{1/2}, \quad (4.11)$$

where the dispersion due to the AF exchange J_{ab} coupling in ab planes depends on the two-dimensional structure function,

$$\gamma(\mathbf{k}) = \frac{1}{2}(\cos k_x + \cos k_y). \quad (4.12)$$

The two branches of $\omega_{O\pm}(\mathbf{k})$ follow from the alternating FM $J_{c1} < 0$ Eq. (4.3) and AF $J_{c2} > 0$ Eq. (4.4) exchange interactions along the c axis in a dimerized OVB state, shown in Fig. 3(a). For the case of $\eta = 0$ the spin waves extend up to $\sim 1.62J$ (Fig. 5).

For the G -AF phase one finds the spin waves which depend on the (weakly anisotropic) AF exchange interactions given by Eqs. (4.7) and (4.8),

$$\omega_G(\mathbf{k}) = 2 \left\{ (2J_{ab} + J_c)^2 - (2J_{ab}\gamma_{\mathbf{k}} + J_c \cos k_z)^2 \right\}^{1/2}. \quad (4.13)$$

For the numerical evaluation we ignored weak anisotropy of the magnetic exchange constants which follows from the spin-orbital model, and adopted the experimental isotropic parameters $J_{ab} = J_c = 5.7$ meV, i.e., $J_{ab} = J_c = 0.1425J$ for $J = 40$ meV.³⁶ These parameters are somewhat lower than those which would result from Eqs. (4.7) and (4.8) for the present value of J at $\eta = 0.13$, and give the width of the magnon dispersion close to $0.85J$, see Fig. 6(a).

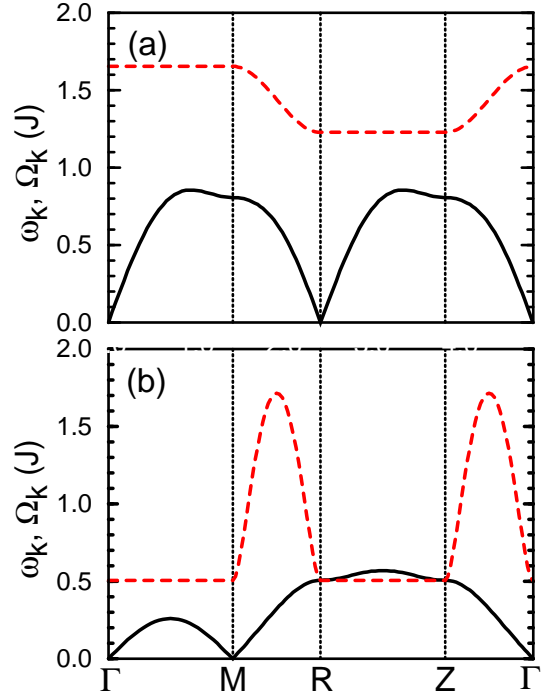


FIG. 6: (Color online) Spin-wave dispersions $\omega_{\mathbf{k}}$ (full lines) as obtained in the LSW theory for the parameters motivated by experiment³⁶ (for $J = 40$ meV): (a) G -AF phase with $J_{ab} = 0.1425J$ and $J_c = -0.1425J$; (b) C -AF phase with $J_{ab} = 0.0650J$ and $J_c = 0.0775J$. Orbital excitations $\Omega_{\mathbf{k}}$ (dashed lines) were obtained within the LOW theory for the G -AF phase (a), and for a disordered orbital state in C -AF phase (b). Other parameters: $\eta = 0.13$, $V_a = 0.3J$, $V_c = 0.84J$. High symmetry points as in Fig. 5.

Finally, we consider the C -AF phase with uniform FM interactions J_c for which one finds the spin-wave dispersion (for more details see Appendix B)

$$\omega_C^{(0)}(\mathbf{k}) = 2 \left\{ [2J_{ab} + |J_c|(1 + \cos k_z)]^2 - (2J_{ab}\gamma_{\mathbf{k}})^2 \right\}^{1/2}. \quad (4.14)$$

This result corresponds to an idealized structure when the observed alternation of stronger and weaker FM interactions along the c axis (see Sec. VB) is ignored. Taking again the experimental exchange constants:³⁶ $J_{ab} = 2.6$ meV and $J_c = 3.1$ meV, i.e., $J_{ab} = 0.065J$ and $J_c = 0.077J$ for $J = 40$ meV, one finds that the spin wave spectrum extends up to $0.57J$, see Fig. 6(b). Therefore, due to the observed strong reduction of the exchange interactions,³⁶ the overall width of the magnon band is *lower* in C -AF phase, while the theory predicts³¹ here a *wider* magnon band for rather similar exchange interactions in both C -AF and G -AF phase, as they follow from Eq. (2.9).

C. Orbital excitations

In contrast to spins which show particular types of long range order in various phases of Fig. 3, the orbitals are in the first instance disordered due to a robust tendency towards strong 1D fluctuations of a and b orbitals along c axis.^{57,58} This may change, however, when lattice distortions [which induce intersite orbital interactions in \mathcal{H}_{orb} in Eq. (2.18)] contribute and stabilize a particular type of AO order. Therefore, one has to employ different approaches to determine the orbital excitations — they depend on the parameter regime and on the underlying orbital phase.

First, in the OVB phase the orbitals are entirely disordered, and one has only the short range order of orbital singlets along c axis which imposes the dimerized magnetic phase, see Fig. 3(a). Under these circumstances, one finds an orbital triplet excitation for each singlet bond along c axis which supports local FM spin order,

$$\Omega_O(\mathbf{k}) = J\left(r_1 + \frac{1}{4}v_c\right). \quad (4.15)$$

As these orbital excitations are local, they are dispersionless and involve no further quantum correction to the energy E_{OVB} given by Eq. (3.3).

Second, although we will show below that a and b orbitals are to some extent disordered in C -AF phase, weak long range order survives in the relevant range of parameters near $\eta \sim 0.13$, so we may start with a classical G -AO order at $T = 0$, and make an expansion around this state using Gaussian fluctuations. In this approach one rotates first the orbital operators on the sites occupied by b orbitals (down pseudospins) with $\langle \tau_i^z \rangle = -\frac{1}{2}$ by angle π with respect to pseudospin x axis, which leads to the canonical transformation:

$$\tau_i^\pm \Rightarrow -\tau_i^\pm, \quad \tau_i^z \Rightarrow -\tau_i^z. \quad (4.16)$$

Next we introduce a similar expansion to that considered above for the spin operators,⁴² and express the orbital operators in terms of the respective Holstein-Primakoff bosons $\{b_i, b_i^\dagger\}$,

$$\tau_i^+ \simeq b_i, \quad \tau_i^- \simeq b_i^\dagger, \quad \tau_i^z = \frac{1}{2} - b_i^\dagger b_i. \quad (4.17)$$

Here we assumed a robust G -type OO (G -AO) state which may be used as a classical state to determine the orbital excitations by performing a Gaussian expansion around it. When only the leading terms are kept within the LOW theory,⁵⁹ one finds after the Fourier transformation and the subsequent Bogoliubov transformation the orbital-wave energy,

$$\Omega_C^{(0)}(k_z) = J\{\Delta^2 + r_1^2 \sin^2 k_z\}^{1/2}. \quad (4.18)$$

The spectrum has a gap at $k_z = 0$

$$\Delta = \left\{ [\eta(r_1 + r_3) + v_0] [2r_1 + \eta(r_1 + r_3) + v_0] \right\}^{1/2} \quad (4.19)$$

at $k_z = 0$, where

$$v_0 = 2v_a - v_c. \quad (4.20)$$

Note that the gap Δ depends on a linear combination of orbital interactions v_0 for the present form of Eq. (2.19), so the interactions along c axis and the ones in ab planes partly compensate each other in Eq. (4.20). In fact, Eq. (4.18) reproduces the earlier result obtained for $v_0 = 0$ in Ref. 42, but in general both types of orbital interactions originate from different distortions and are thus independent from each other. The orbiton dispersion demonstrates that the present phase is stable at finite η only as long as $\Delta > 0$, i.e., in a range of $v_0 > -\eta(r_1 + r_3)$. The orbital-wave dispersion (4.18) follows from the quantum fluctuations along the c axis, and thus depends only on the z th momentum component k_z . We emphasize that the orbital excitations are typically at higher energy than the spin excitations as the orbital gap Δ is finite, see Fig. 6(b).

Here we also give the values of the orbital correlations which enter Eqs. (4.1) and (4.2). It is convenient to introduce the following integrated quantities:

$$s_1 = \frac{1}{2N} \sum_k \left\{ A - \Omega_C^{(0)}(k) \right\}, \quad (4.21)$$

$$s_2 = \frac{1}{2N} \sum_k \left\{ \frac{A}{\Omega_C^{(0)}(k)} - 1 \right\}, \quad (4.22)$$

where $A = r_1 + 2\eta(r_1 + r_3)\langle \tau^z \rangle$. The orbital correlations and the OO parameter,

$$\langle \tau^z \rangle = \frac{1}{2} - s_2, \quad (4.23)$$

are reduced by quantum fluctuations along the c axis and are determined self-consistently. One finds that weak OO appears at finite $\eta > 0.08$ (at $\eta < 0.08$ the orbitals are disordered and $\langle \tau^z \rangle = 0$), and $\langle \tau^z \rangle \simeq 0.26$ for $\eta = 0.13$, i.e., the OO is only about *half of the classical value* for the realistic parameters of cubic vanadates.¹⁰ This demonstrates that the $\{a, b\}$ orbitals strongly fluctuate and the G -AO order is rather weak. Strong orbital fluctuations can be also verified by calculating the intersite orbital correlations:

$$\langle \vec{\tau}_i \cdot \vec{\tau}_j \rangle = -\frac{1}{4} - \frac{1}{r_1} [s_1 + \eta(r_1 + r_3)s_2]. \quad (4.24)$$

Indeed, one finds a rather low value of $\langle \vec{\tau}_i \cdot \vec{\tau}_j \rangle \simeq -0.428$ (not so far from the Bethe ansatz result -0.4431 for the AF Heisenberg chain), and the dominating contribution comes not from the static term $\langle \tau_i^z \tau_j^z \rangle = -\langle \tau^z \rangle^2 \simeq -0.068$, but from the fluctuating part, $\langle \tau_i^x \tau_j^x + \tau_i^y \tau_j^y \rangle \simeq -0.36$.

Finally, the opposite situation is found in the G -AF phase, where structural distortions observed below T_{N2} suggest that the C -AO order sets up. In this case the a and b orbitals repeat each other along the chains in c

direction, and alternate in ab planes [Fig. 3(c)]. This robust C -type orbitally ordered state may be used to determine the orbital excitations employing the LOW theory.⁵⁹ We used again a rotation of 'down' pseudospins as in Eq. (4.16) in order to obtain a uniform ferro-orbital state, and next expressed the orbital operators in terms of the Holstein-Primakoff bosons $\{b_i, b_i^\dagger\}$, using Eqs. (4.17). By applying a similar procedure to that used above for the G -AO phase, i.e., keeping only bilinear terms in the leading LOW order, and employing subsequent Fourier and Bogoliubov transformations, this leads to the orbital waves in the C -AO phase, with dispersion

$$\Omega_G(\mathbf{k}) = J(\eta r_1 \cos k_z + v_c + 2v_a), \quad (4.25)$$

characterized by a large gap of $\sim (V_c + 2V_a)$, shown in Fig. 6(a). We emphasize that the interactions with the lattice are here of crucial importance and generate a large gap, while the orbital gap found in the C -AO phase follows predominantly from the superexchange interactions and is therefore typically much smaller than the one in the G -AO phase.⁶⁰

D. Zero temperature phase diagram

In order to investigate the relative stability of the magnetic phases shown schematically in Fig. 3, one has to determine the quantum corrections due to magnetic and orbital excitations. The quantum corrections due to orbital fluctuations were already included in the energies of the OVB (3.3) and C -AF (3.4) phases, where the orbital singlets along c axis dominate and are responsible either for the orbital disordered state or for weak G -AO order, respectively. The quantum correction to the energy of the G -AF phase due to the almost dispersionless orbital waves Eq. (4.25) is rather small and will be neglected below.⁶¹

The remaining quantum corrections to the classical energy of the Néel state due to spin excitations can be found using the standard approach of the LSW theory. At $T = 0$ the total energy,

$$E_M = E_M^{(0)} - \delta E_M, \quad (4.26)$$

is lowered by the quantum fluctuation contribution³¹

$$\delta E_M = 2J_{ab} + |J_c| - \frac{1}{2(2\pi)^3} \int d^3\mathbf{k} \omega_M(\mathbf{k}), \quad (4.27)$$

where label $M = 0, C, G$ stands for a given magnetic phase considered here, either OVB, or C -AF, or G -AF; while $\omega_M(\mathbf{k})$ in Eq. (4.27) is the spin wave dispersion in this phase. We have evaluated quantum corrections using Eq. (4.27) for all three magnetic phases: OVB, C -AF and G -AF. It is instructive to investigate first the energy dependence on Hund's exchange interaction, shown in Fig. 7. As the quantum corrections which result from spin excitations are similar for all three AF phases, the

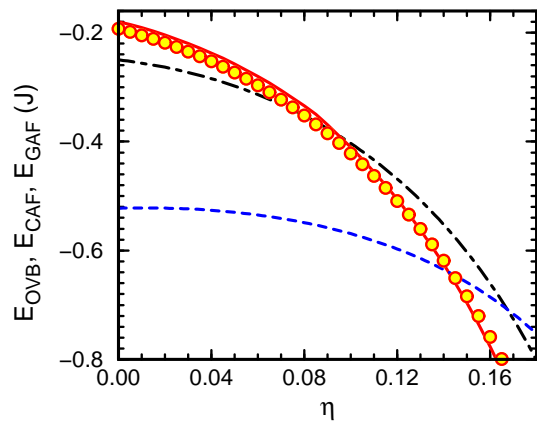


FIG. 7: (Color online) Energies of different phases for increasing Hund's exchange η : C -AF phase (solid line), OVB phase (dashed-dotted line), and G -AF phase (long-dashed line). The energy of the G -AF phase is shown for $2V_a = V_c = 0.45J$ (the other energies do not depend on V_c). A constant energy term $-2J$ was neglected in all phases. The circles show for a comparison the energy obtained for decoupled FM chains along c axis, with orbital correlations described by the 1D pseudospin Heisenberg model.

qualitative picture obtained with these corrections and presented in Sec. III B is confirmed: the C -AF is stable in a range of realistic values of Hund's exchange $\eta \sim 0.13$ for small orbital interaction parameter V_c , while increasing this interaction results in a transition to the G -AF phase, where the magnetic energy is gained on all the bonds after the orbitals have reoriented to the C -AO order, see Fig. 3.

A transition from the OVB phase to the C -AF one under increasing η is rather intricate. At small values of η when the OVB phase is still stable, the competing phase with C -AF spin order is the orbital disordered phase, as the orbital superexchange interactions in ab planes are so weak (and the orbital interactions cancel each other on the mean field level for $2V_a = V_c$) that the 1D pseudospin interaction along the c axis dominates⁵⁷ the behavior of the orbital chain (see Fig. 7). However, at $\eta \sim 0.13$ one finds that weak G -AO order is stabilized by Ising orbital interactions along the bonds in ab planes. However, the orbital fluctuations are still very strong in this state as described in Sec. IV C. Of course, the G -AO order could be further stabilized and become of more classical character³⁴ when $2V_a > V_c$, but this picture of the C -AF phase contradicts recent experiments.³⁰

By comparing energies of all three magnetic phases at $T = 0$ one finds the phase diagram of Fig. 8. To simplify the discussion we have adopted here the parametrization $V_c = 2V_a = 2V$. In fact, one expects that the GdFeO₃-like distortions are responsible for stronger orbital interactions along c axis, and the parameter V_c plays a more important role (than V_a) in stabilizing the C -AO order which supports the G -AF spin order. The OVB phase is stable for small values of η and V , while for sufficiently

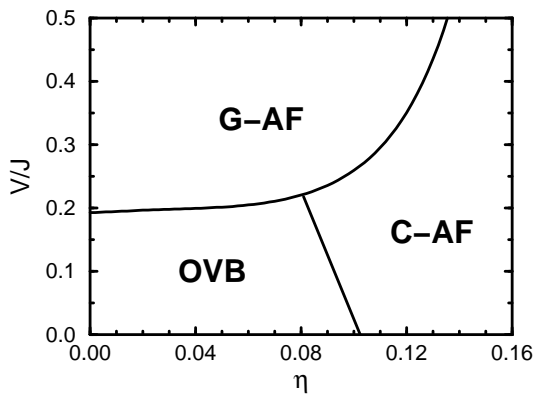


FIG. 8: Mean-field phase diagram of the spin-orbital model (2.18) as obtained for cubic vanadates in the (η, V) plane at $T = 0$ for $V_c = 2V_a = 2V$. At the spectroscopic value of $\eta \simeq 0.13$ two phases are possible: C -AF phase (for $V < V_0$) and G -AF phase (for $V > V_0$), with $V_0 \simeq 0.43J$; these two AF states are observed at low temperature in LaVO_3 (C -AF) and in YVO_3 (G -AF), respectively.

large V the G -AF phase takes over. At larger values of η two AF phases observed in the cubic vanadates,³⁰ C -AF and G -AF phase, compete with each other. The range of stability of the C -AF phase increases with increasing η as the FM interaction along c axis is then enhanced, see Fig. 4(b). In contrast, both AF exchange interactions in the G -AF phase are reduced, so this phase has to be stabilized by larger orbital interaction V .

V. SCENARIO FOR YVO_3

A. Peierls orbital dimerization

Before we address the experimental situation in YVO_3 , we demonstrate an intrinsic instability of the 1D spin-orbital chain towards dimerization.⁵⁷ In contrast to the 1D Heisenberg antiferromagnet with fixed exchange interactions on each bond $\langle i, i+1 \rangle$, the orbital interaction in the present case are [in the leading order, see Eq. (2.11)] given by

$$J_{\text{orb}}(i, i+1) = \frac{1}{2}(1 + 2\eta r_1) \langle \vec{S}_i \cdot \vec{S}_{i+1} + 1 \rangle, \quad (5.1)$$

i.e., for each bond the orbital interaction is tuned by the spin correlation function on this bond. While at temperature $T = 0$ the spins are (almost) fully polarized and $\langle \vec{S}_i \cdot \vec{S}_{i+1} \rangle \simeq 0.96$,³¹ the spin correlations could in principle alternate between stronger and weaker FM bonds at finite temperature $T > 0$, and then the orbital interaction would be modulated as follows

$$J_{\text{orb}}(i, i+1) = J_o(1 \pm \delta_o), \quad (5.2)$$

between even and odd bonds. Note that J_o stands here for the average value that will gradually decrease with

increasing temperature. This additional temperature dependence complicates somewhat the picture of the C -AF phase.

Assuming the alternating orbital interactions (5.2) and performing the transformation to fermions for the corresponding XY model in the orbital sector, one finds the following spinless fermion problem using the Jordan-Wigner transformation⁶²

$$\mathcal{H}_{XY}(\delta_o) = \frac{1}{2} J_o \sum_i (1 \pm \delta_o) (f_i^\dagger f_{i+1} + f_{i+1}^\dagger f_i). \quad (5.3)$$

The diagonalization of Hamiltonian (5.3) gives the energy spectrum of a dimerized fermionic chain,

$$\varepsilon_{\pm}(k) = \pm \sqrt{\cos^2 k + \delta^2 \sin^2 k}, \quad (5.4)$$

and the total energy at $T = 0$:

$$E(\delta_o) = -J_o \frac{3}{2\pi} \int_0^{\pi/2} dk \varepsilon_-(k). \quad (5.5)$$

The energy $-0.4776J$ obtained from Eq. (5.5) at $\delta_o = 0$ is slightly lower than the Bethe ansatz result ($-0.4431J$), while at $\delta_o = 1$ the exact result found for the orbital singlets on every second bond is rigorously reproduced. Therefore, Eq. (5.5) may be considered to be a reasonable interpolation formula which allows one to investigate the dimerized orbital chain in the entire regime of δ_o . While an average value of the orbital correlation function $\langle \vec{\tau}_i \cdot \vec{\tau}_{i+1} \rangle$ increases with δ_o , the chain with a constant exchange interaction cannot dimerize by itself. In contrast, the energy $E(\delta_o)$ indeed decreases when the alternation of the orbital interactions (5.2) is allowed, so the chain does have a tendency to dimerize (Fig. 9).

It is quite remarkable that already a weak anisotropy δ_o in orbital interactions is sufficient to give rather different orbital correlations $\langle \vec{\tau}_i \cdot \vec{\tau}_{i+1} \rangle$ on even/odd bonds. These different orbital correlations can trigger the alternation in the spin correlation functions, and in this way the dimerized state could be a self-consistent solution of the spin-orbital problem at finite temperature. We emphasize that even a relatively small anisotropy $\delta_\tau = 0.12$ in the orbital correlations,

$$\delta_\tau = |\langle \vec{\tau}_i \cdot \vec{\tau}_{i+1} \rangle - \langle \vec{\tau}_{i+1} \cdot \vec{\tau}_{i+2} \rangle|, \quad (5.6)$$

is already sufficient to generate considerable anisotropy in the magnetic exchange constants J_{c1} and J_{c2} along c axis (Fig. 10). The exchange constants of Fig. 10 were obtained with $J = 30$ meV — this reduction of the energy scale by a semiempirical factor of 0.75 from that given by the analysis of the optical spectrum¹⁰ was necessary as otherwise the model (2.18) would predict too large exchange constants for the G -AF phase. Furthermore, we note that the above anisotropy δ_τ is obtained already with $\delta_o = 0.017$ when the mapping to the fermion problem (5.3) is used (Fig. 9). Of course, this problem requires a self-consistent solution at finite temperature as we discuss in Sec. VB.

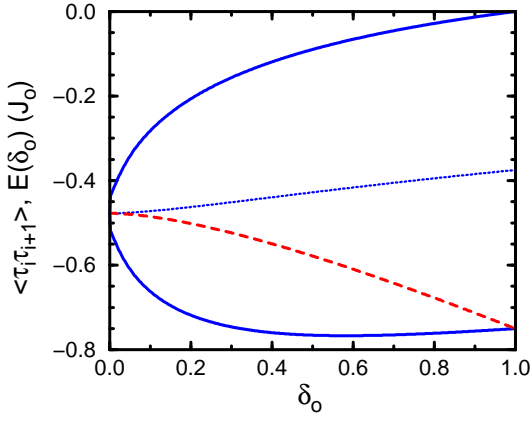


FIG. 9: (Color online) Orbital correlation functions $\langle \vec{\tau}_i \cdot \vec{\tau}_{i+1} \rangle$ at even and odd bonds along a dimerized 1D chain, as obtained within the XY model for increasing anisotropy δ_o in the exchange constants, see Eq. (5.2). The energy $E(\delta_o)$ (dashed line), obtained using spinless fermions Eq. (5.5), decreases with increasing δ_o , while the average energy in an orbital chain with the same exchange interaction J_o at each bond would increase (dotted line).

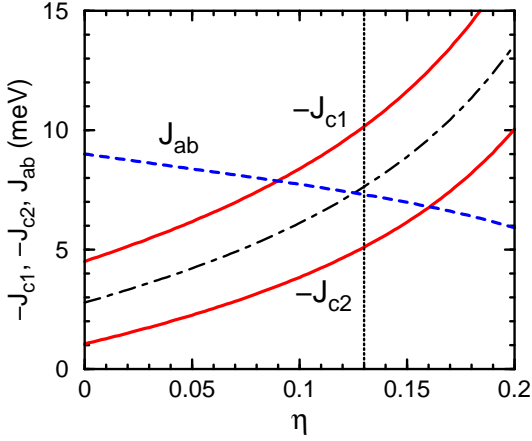


FIG. 10: (Color online) Exchange constants J_{ab} (dashed line), J_{c1} and J_{c2} (solid lines), all in meV, as obtained for the idealized C -AF phase with condensed xy orbitals ($n_c = 1$), Eqs. (2.8), and orbital disordered state along c axis with dimerized orbital correlations. Vertical line indicates the value of $\eta = 0.13$ estimated from the atomic data⁴⁷ and from the optical data¹⁰ for LaVO_3 . Parameters: $J = 30$ meV, $\langle \vec{\tau}_i \cdot \vec{\tau}_{i+1} \rangle = -0.4431$, $\delta_\tau = 0.12$ (5.6).

B. Reduction of exchange constants by orbital fluctuations

Although the value of $J \sim 40$ meV deduced from the neutron scattering data³⁶ for YVO_3 gives a consistent description of the temperature dependence of the optical spectral weight for the high-spin excitations along c axis in LaVO_3 , there is a fundamental problem concerning the size of magnetic exchange constants, particularly in the

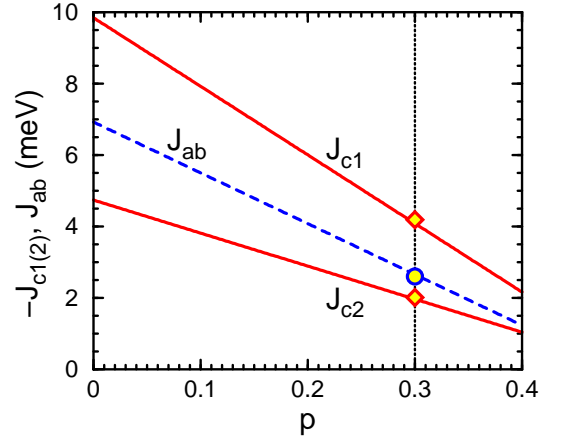


FIG. 11: (Color online) Reduction of exchange constants J_{ab} (dashed line), J_{c1} and J_{c2} (solid lines), all in meV, in the dimerized C -AF phase due to orbital bond fluctuations between FM and AF bonds, as given by Eqs. (5.7)–(5.9). Orbital disordered state along c axis is assumed at $p = 0$. Experimental values of exchange constants found for the C -AF phase of YVO_3 ,³⁶ shown by circle ($J_{ab} \simeq 2.6$ meV) and by diamonds ($J_{c1} \simeq 4.2$ meV and $J_{c2} \simeq 2.0$ meV), are nearly reproduced for moderate fluctuations with $p = 0.30$ (vertical dashed line). Parameters: $J = 30$ meV, $\eta = 0.13$, $\delta_s = 0.35$.

exotic C -AF phase of YVO_3 , stable in the intermediate temperature range $T_{N2} < T < T_{N1}$. First of all, the calculations performed using the mean-field approach and assuming rigid OO (see Fig. 3), as in Ref. 9, predict too large exchange constants in both phases when $J = 40$ meV is assumed. In fact, for the G -AF phase one finds then the values of both J_c and J_{ab} being larger by $\sim 25\%$ than the respective experimental values of Ulrich *et al.*³⁶ Moreover, in experiment one finds an (almost) isotropic G -AF phase with $J_c = J_{ab}$, while the present model predicts (except at small $\eta < 0.10$) an anisotropy between c axis and ab planes, with $J_c > J_{ab}$, see Eqs. (4.7) and (4.8). This suggests that already for the G -AF phase some 'dynamical' reduction mechanism of the magnetic exchange constants is at work, which we simulate by reducing the superexchange energy scale down to $J \sim 30$ meV. Indeed, taking an average value of the magnetic exchange constants over three cubic directions we arrive then at the experimental result $J_c = J_{ab} \sim 5.7$ meV.

While the above procedure could be still considered as a fair agreement between the theoretical model and experiment, it is surprising that the magnetic exchange constants in the C -AF phase cannot be obtained from the model using the same parameters. In fact, the values of J_c and J_{ab} shown in Fig. 10 for $\eta = 0.13$ are by almost a factor of 2 larger than those deduced from the neutron scattering data at 85 K.³⁶ This strongly suggests that some of the assumptions used so far to derive the values of J_c^C and J_{ab}^C from Eqs. (4.1) and (4.2) have to be reconsidered.

One of the most puzzling experimental features in

YVO₃ is the nature of the structural transition at T_s , which removes the orbital degeneracy and induces the splitting Δ between the xy orbitals and the yz/zx doublet, see Fig. 1. We anticipate that this splitting is not large enough to impose strict freezing of charge in xy orbitals. Thus we expect that some orbital fluctuations should still be present in the intermediate temperature regime $T_{N2} < T < T_s$ before the orbitals undergo the transition into the C -AO phase (supporting G -AF spin order) below T_{N2} , as shown in Fig. 3(c).

Qualitatively, we illustrate the consequences of orbital fluctuations on the magnetic exchange constants by considering a plaquette which includes two bonds along c axis and two other bonds along either a or b axis. If the c orbitals are occupied at each site, and a/b orbitals fluctuate, a representative state of such a plaquette contains 4 electrons in c orbitals, and 2 in each of two other states, a and b . The effective superexchange Hamiltonian (2.9) contains the terms with double orbital excitations on the bonds, $\propto \tau_i^\pm \tau_j^\pm$, see Eq. (2.16). Such terms on the bonds along a (or b) axis generate a/b orbital configurations on each site i and j . Only one of these two orbitals (a or b) is active along this particular bond, and it resembles the bond along c axis before the orbital fluctuation took place. As a result, such fluctuations lead to (locally) FM contributions in the ab planes, and to (locally) AF contributions along c axis — both of them will reduce the actual values of J_c^C and J_{ab}^C exchange constants.

Following the above idea, we introduce *effective* magnetic exchange constants,

$$\mathcal{J}_{c1}^C = (1 + \delta_s)[(1 - p)J_c^C(0) + pJ_{ab}^C(0)], \quad (5.7)$$

$$\mathcal{J}_{c2}^C = (1 - \delta_s)[(1 - p)J_c^C(0) + pJ_{ab}^C(0)], \quad (5.8)$$

$$\mathcal{J}_{ab}^C = (1 - p)J_{ab}^C(0) + pJ_c^C(0), \quad (5.9)$$

as a superposition of two contributions obtained for the undimerized state without xy orbital fluctuations (for $n_c = 1$), $J_c^C(0)$ and $J_{ab}^C(0)$, calculated as described in Sec. IV A. The probabilities $(1 - p)$ and p refer to the initial state with c orbitals occupied ($n_c = 1$), and to the configuration with flipped orbitals after the plaquette fluctuation has occurred ($n_c = 0$), respectively. The result of the numerical calculation for the usual parameters shows that one arrives almost at experimental values of the magnetic exchange constants when moderate orbital fluctuations with $p = 0.30$ considerably reduce the exchange constants (see Fig. 11). For the experimental anisotropy δ_s one finds large alternation of the FM exchange constants along c axis with respect to the average value,

$$\mathcal{J}_c^C = (1 - p)J_c^C(0) + pJ_{ab}^C(0). \quad (5.10)$$

Next, we analyze the spin excitations in the dimerized C -AF phase in order to calculate the spin correlations, the quantum fluctuation correction to the ground state energy (see Appendix B), as well as the free energy at finite temperature, see Sec. V C. The effective spin

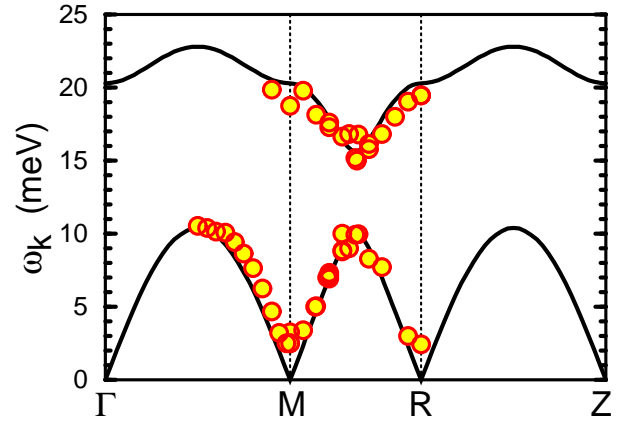


FIG. 12: (Color online) Spin-wave dispersions $\omega_{\mathbf{k}}$ (full lines) as obtained in the LSW theory along the representative directions in the Brillouin zone for the dimerized C -AF phase with experimental exchange constants:³⁶ $J_{ab} = 2.6$ meV, $J_c = 3.1(1 \pm \delta_s)$ meV and $\delta_s = 0.35$. These interactions are obtained by considering plaquette fluctuations of spin exchange interactions as described in the text (see also Fig. 11). Parameters: $J = 30$ meV, $\eta = 0.13$, $\delta_s = 0.35$, $p = 0.30$. The experimental points of Ref. 36 measured by neutron scattering at $T = 85$ K are reproduced by circles (the effective linewidths are not shown). The high symmetry points are: $\Gamma = (0, 0, 0)$, $M = (\pi, \pi, 0)$, $R = (\pi, \pi, \pi)$, $Z = (0, 0, \pi)$.

Hamiltonian for this phase is given as follows:

$$\begin{aligned} \mathcal{H}_s = & \mathcal{J}_c^C(1 + \delta_s) \sum_{\langle 2i, 2i+1 \rangle \| c} \vec{S}_{2i} \cdot \vec{S}_{2i+1} \\ & + \mathcal{J}_c^C(1 - \delta_s) \sum_{\langle 2i-1, 2i \rangle \| c} \vec{S}_{2i-1} \cdot \vec{S}_{2i} \\ & + \mathcal{J}_{ab}^C \sum_{\langle ij \rangle \| ab} \vec{S}_i \cdot \vec{S}_j. \end{aligned} \quad (5.11)$$

Following the LSW theory, the spin wave dispersion is given by

$$\begin{aligned} \omega_{C\pm}(\mathbf{k}) = & 2 \left\{ [2\mathcal{J}_{ab} + |\mathcal{J}_c| \right. \\ & \left. \pm \mathcal{J}_c(\cos^2 k_z + \delta_s^2 \sin^2 k_z)^{1/2}]^2 - (2\mathcal{J}_{ab}\gamma_{\mathbf{k}})^2 \right\}^{1/2}. \end{aligned} \quad (5.12)$$

For the numerical evaluation of Fig. 12 we have used the experimental exchange interactions:³⁶ $\mathcal{J}_{ab} = 2.6$ meV, $\mathcal{J}_c = 3.1$ meV, $\delta_s = 0.35$. Indeed, large gap is found between two modes halfway in between the M and R points, and between the Z and Γ points (not shown), respectively. Two modes measured³⁶ and obtained from the present theory in the unfolded Brillouin zone follow from the dimerized magnetic structure.

The microscopic reason of the anisotropy in the exchange constants \mathcal{J}_{c1} and \mathcal{J}_{c2} is the tendency of the orbital chain to dimerize, as we have demonstrated in Sec. V A. Such a dimerized orbital chain may only be stable,

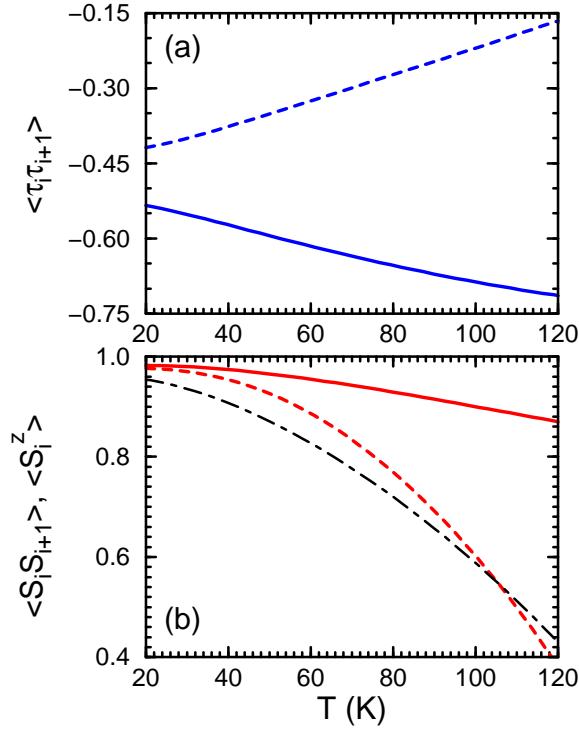


FIG. 13: (Color online) Result of the self-consistent calculation of intersite correlations in the dimerized C -AF phase along c axis for increasing temperature: (a) orbital $\langle \vec{\tau}_i \cdot \vec{\tau}_{i+1} \rangle$, and (b) spin $\langle \vec{S}_i \cdot \vec{S}_{i+1} \rangle$. The correlations on stronger (weaker) FM bonds are shown by solid (dashed) lines. Dashed-dotted line in (b) shows the order parameter $\langle S^z \rangle$ in the C -AF phase as obtained from the LSW theory. Parameters: $\eta = 0.13$, $J = 30$ meV, and $p = 0.30$, see Fig. 11.

however, if the corresponding interactions in the orbital sector (5.2) alternate, i.e., $\delta_o > 0$. This becomes possible at finite temperature when also intersite spin correlations may alternate along the c axis, supporting such a dimerized state. Although a completely satisfactory treatment of the spin correlations in a broad temperature regime which covers the symmetry broken C -AF phase is not possible at the moment, we have employed the LSW theory to calculate the spin correlations $\langle \vec{S}_i \cdot \vec{S}_{i+1} \rangle$, as explained in the Appendix B.

The result of the self-consistent calculation of spin and orbital correlations along the c axis in the dimerized C -AF phase is shown in Fig. 13. The driving force to stabilize the dimerized state is the instability of the orbital chain which leads to rather strong anisotropy in the orbital correlations [Fig. 13(a)]. On the contrary, the spin correlations differ only by a rather small amount (unlike in the OVB phase), as the large spins $S = 1$ are far less susceptible to follow the dimerized structure, and the long range spin order is supported by the exchange interactions in all three directions. The energy of the dimerized state is lower than that of the undimerized C -AF structure. Apparently, a weak anisotropy between

$\langle \vec{S}_i \cdot \vec{S}_{i+1} \rangle \sim 0.93$ and ~ 0.79 on stronger/weaker FM bonds encountered at $T = 77$ K [see Fig. 13(b)] is already sufficient to trigger a phase transition to this phase from the G -AF phase stable below T_{N2} . Why this transition may really happen in YVO_3 we explain in the following Section.

C. Mechanism of the phase transition from G -AF to C -AF phase

The transition from G -AF to C -AF phase in YVO_3 is puzzling as the magnetic order changes completely at finite temperature $T_{N2} \simeq 77$ K, and the magnetic moments reorient.³³ The observed change of the spin and orbital pattern indicates that the spin-orbital superexchange interactions are frustrated and it is easy to tip the balance of these interactions and to change completely both the magnetic and orbital order. As the transition between the two phases occurs at finite temperature, the entropy has to play an important role, so it was suggested before that the large orbital entropy due to orbital fluctuations in the C -AF phase could be released at T_{N2} and trigger the transition.⁴² A closer inspection of the present model and the reconsideration of recent experiments show, however, that the situation is somewhat more intricate.

First of all, we have already emphasized that the magnetic exchange constants are reduced in the C -AF phase, and we presented a possible mechanism responsible for this reduction in Sec. VB. As a result of orbital fluctuations, the average energy of magnetic excitations is lowered in the C -AF phase (Fig. 6), so one expects that the *spin entropy* might play an important role as well. Using the spin and orbital excitations derived already for both phases in the previous Sections, we estimate these entropy contributions assuming that the excitations are independent from each other. The spin waves are given by Eqs. (4.13) and (5.12), while the orbital excitations by Eqs. (4.25) and (4.18). Here we will ignore the change of the orbital excitations in the dimerized C -AF phase as this gives only a marginal contribution to the entropy of the C -AF phase, and does not influence the magnetic transition at T_{N2} significantly.

The spin and orbital entropy normalized per one vanadium ion is calculated using standard formulae:

$$\begin{aligned} \mathcal{S}_C = & k_B T \frac{1}{2N} \sum_{\mathbf{k}} \left\{ \log \left(1 - e^{-\beta \omega_{C+}(\mathbf{k})} \right) \right. \\ & \left. + \log \left(1 - e^{-\beta \omega_{C-}(\mathbf{k})} \right) \right\} \\ & + k_B T \frac{1}{N_1} \sum_{\mathbf{k}} \log \left(1 - e^{-\beta \Omega_C(k)} \right), \end{aligned} \quad (5.13)$$

$$\begin{aligned} \mathcal{S}_G = & k_B T \frac{1}{N} \sum_{\mathbf{k}} \left\{ \log \left(1 - e^{-\beta \omega_G(\mathbf{k})} \right) \right. \\ & \left. + k_B T \frac{1}{N_1} \sum_{\mathbf{k}} \log \left(1 - e^{-\beta \Omega_G(k)} \right) \right\}, \end{aligned} \quad (5.14)$$

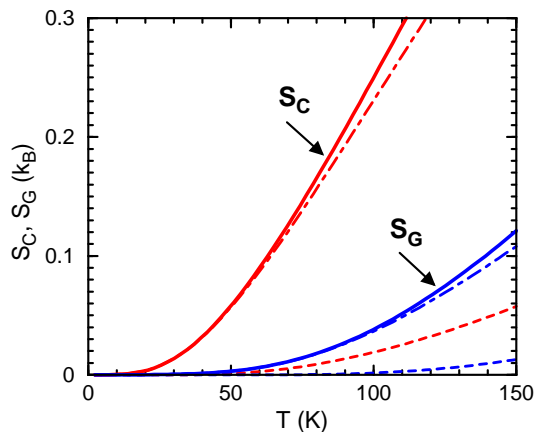


FIG. 14: (Color online) Entropy of the C -AF (S_C) and G -AF (S_G) phase as obtained for the spin-orbital model (2.18) using the experimental values of magnetic exchange constants in both phases. The dominating contributions result from spin excitations (dashed-dotted lines), while the orbital contributions (dashed lines) are much smaller, but give also a higher entropy in the C -AF phase. Parameters: $J = 40$ meV, $\eta = 0.13$, $V_a = 0.30J$, $V_c = 0.84J$.

where $\beta = 1/k_B T$, and N (N_1) is the number of \mathbf{k} (k) values. The entropy consists of the spin and orbital terms for each phase. All summations are over the Brillouin zone which corresponds to the undimerized C -AF phase. Using the parameters consistent with the experimental data of Ulrich *et al.*³⁶ one finds (see Fig. 14) that: (i) the entropy S_C for the C -AF phase is larger than S_G for the G -AF phase, and (ii) the spin entropy grows significantly faster with temperature than the orbital entropy for each phase. Therefore, we conclude that the spin entropy gives here a more important contribution and decreases the difference between the free energies of both magnetic phases in the temperature range $T \sim T_{N2}$.

It has been argued before^{8,42} that the difference between the energies of both phases, E_G and E_C , has to be small at $T = 0$. Indeed, we evaluated the free energy of both phases using the above entropies (5.13) and (5.14),

$$\mathcal{F}_C = E_C - T S_C, \quad (5.15)$$

$$\mathcal{F}_G = E_G - T S_G, \quad (5.16)$$

and found that $E_C - E_G \simeq 1$ meV, and the transition from G -AF to C -AF phase is reproduced at the experimental value of the temperature T_{N2} when the orbital interactions are chosen properly. In Fig. 15 we show a representative case with $V_a = 0.30J$, $V_c = 0.84J$ with $J = 40$ meV. Of course, this fit is not unique and V_a (V_c) could be somewhat smaller (larger), but the energy difference $E_C - E_G$ at $T = 0$ remains close to 1 meV in all cases. Note, however, that too large values of V_c are not allowed, as then the C -AF phase gets destabilized by orbital excitations (4.18).

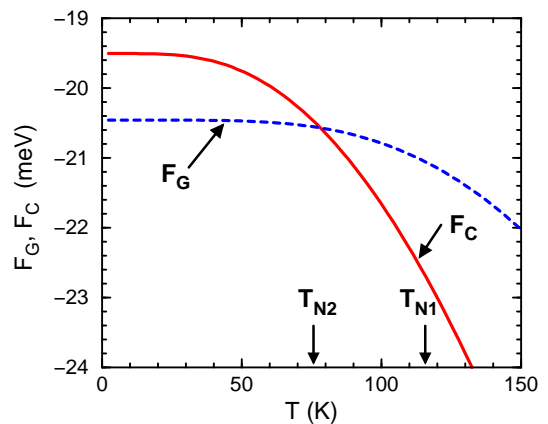


FIG. 15: (Color online) Free energies of the C -AF (\mathcal{F}_C , solid line) and G -AF (\mathcal{F}_G , dashed line) phase as obtained for the spin-orbital model (2.18) using the experimental values of magnetic exchange constants³⁶ in both phases. The experimental magnetic transition temperatures, $T_{N2} \simeq 77$ K and $T_{N1} \simeq 116$ K, are indicated by arrows. Parameters are the same as in Fig. 14.

VI. SUMMARY AND CONCLUSIONS

The present study shows the importance of t_{2g} orbital degrees of freedom in cubic vanadates. We have presented the spin-orbital model for cubic vanadates and analyzed its possible solutions in various parameter regimes, using extensively the decoupling of spin and orbital degrees of freedom. Although the model is more general, we have focused on the solutions which arise in the case of anisotropic occupancy of t_{2g} orbitals, with xy orbitals singly occupied at each site. This state is believed to be realized in cubic vanadates, at least in low temperature phases with magnetic long range order. When Hund's exchange and orbital interactions promoted by the lattice are weak, the superexchange is strongly frustrated and gives a rather exotic dimerized OVB state, with orbital singlets alternating along the c axis and stabilized at every second bond by ferromagnetic spin correlations. In this way, spin and orbital correlations support each other and demonstrate a unique instability of the spin-orbital system towards a dimerized state.^{37,57} This instability turns out to play also an important role at finite temperature in YVO_3 , but in a different regime of parameters where its mechanism is more subtle.

When Hund's exchange or the orbital interactions increase, the OVB ground state is disfavored and a particular type of long range magnetic order emerges instead from the frustrated superexchange interactions in cubic vanadates. These other AF states (C -AF and G -AF phases), as well as the OVB state itself (at low J_H), demonstrate a close interrelation between magnetic and orbital order, with complementary behavior of spin and orbital correlations, known as the so-called Goodenough-Kanamori rules.^{5,54} While in some cases these rules (and

the underlying decoupling of spin and orbital operators) work well, we have presented the case of the C -AF phase with rather disordered orbitals, where it is likely that joint spin-orbital fluctuations also play a role,²¹ and it would be necessary to include them for a more quantitative comparison with experiment.

A detailed analysis of the possible solutions of the spin-orbital superexchange model supplemented by the orbital interactions induced by the lattice demonstrates that two different types of AF order, C -AF and G -AF phase, compete with each other in the parameter regime relevant for YVO_3 . However, the energetic proximity of these two phases in a particular parameter regime could explain possible changes of magnetic order by pressure or magnetic field — when the microscopic parameters are fixed, one or the other phase could be stable at $T \rightarrow 0$. The situation changes at finite temperature, however, when the *spin and orbital excitations* are of importance and may tip the energy balance between given two types of order by the entropy term. In fact, we have shown that this is likely to be the microscopic explanation of the observed first-order phase transition and switching of the magnetic order in YVO_3 at T_{N2} .

Our study has established that the nature of the transition from the G -AF to C -AF phase at T_{N2} observed in YVO_3 is complex and several factors have to come together to trigger it when temperature increases: (i) the presence of active t_{2g} orbital degrees of freedom opens a possibility of two different types of AF order which may compete with each other; (ii) rigidity of the C -AO order in the G -AF phase hampers possible free energy gains when spin or orbital excitations are created (as spin interactions are rather strong and the orbital gap is quite large); (iii) the change of structure observed at T_{N2} not only helps to stabilize the weak G -AO order, but also releases more orbital fluctuations when the *xy orbitals become active* and their occupancy is not fixed — such fluctuations result in turn in fluctuating magnetic exchange constants and lead to the reduction of the characteristic energy scale for the spin excitations, and finally (iv) the spin correlations have to be weakened by increasing temperature to participate in a joint spin-orbital dimerization in the C -AF phase. Thus, the difference between the G -AF and C -AF phase of YVO_3 is much deeper than simply the observed difference in the magnetic order. It is far more important that the *orbital state softens* at the transition at T_{N2} to the C -AF phase and this change happens in a concerted way with the observed reorientation of the magnetic moments. In addition, the intrinsic instability in the orbital sector towards dimerization, which is incompatible with the magnetic order in the G -AF phase and is blocked by spin correlations in the C -AF phase at $T = 0$, becomes possible when the intersite ferromagnetic spin correlations along c axis have been somewhat weakened with increasing temperature.

Although we have suggested a plausible scenario of the observed magnetic phase transition in YVO_3 , the microscopic theory of the C -AF phase at finite temperature

remains still to be constructed. It is not clear at the moment to what extent the xy orbital fluctuations are released in the intermediate magnetic phase and are still present up to the structural transition at $T_s \sim 200$ K (see Fig. 1). It could well be that spin-orbital *entanglement in excited states* plays a role in this temperature regime and prevents reliable evaluation of the magnetic exchange constants in the C -AF phase using the conventional decoupling of spin and orbital operators. Furthermore, it is puzzling whether dimerization also plays a role in reducing the the magnetic order parameter in the C -AF phase which is hard to explain using the spin-wave theory, or the above entanglement is the main reason responsible for this reduction. Note however that it could be argued that the observed orientation of the magnetic moments which are close to lying within the ab planes is enforced by the dimerization in the C -AF phase.

Some other problems remain still open and should be treated in future more complete theory. We note that also in the G -AF phase a considerable reduction of the magnetic order parameter³⁶ goes beyond that expected from the quantum fluctuations.³¹ We believe that the relativistic spin-orbit coupling $\propto \lambda \vec{L}_i \vec{S}_i$ contributes significantly to the magnetic properties in the entire regime of temperature,³⁷ in particular also to the spin correlations in the G -AF phase, and could reduce the observed value of the magnetization. In fact, it would also break the symmetry in the spin space and determine an easy axis for the AF order parameter. In the present study the spin-orbit coupling λ was ignored, as in the considered regime of $J \gg \lambda$ it could lead just to the perturbative corrections of the presented spin and orbital excitations. In contrast, in the regime of $\lambda \sim J$ it would lead to ordering of orbitals with complex coefficients, $(|xz\rangle \pm i|yz\rangle)/\sqrt{2}$, with finite orbital angular momentum.³⁷ Although the cubic vanadates are not in this regime of parameters, finite spin-orbit coupling λ would be crucial for quantitative understanding of spin (and orbital) excitations in the entire parameter regime. This interaction provides another mechanism for the softening of spin excitations in the C -AF phase, which would complement the scenario considered in this paper. We also note that a small G -like magnetization component was observed as well in the C -AF phase in the temperature range $T_{N2} < T < T_{N1}$. Therefore, it is likely that this magnetic phase is still more complex than suggested in the present paper, and requires a more careful analysis. Recent progress in experimental methods makes it possible to measure also orbital excitations,^{63,64} and information on the orbital excitations in YVO_3 would be instrumental to resolve some of the above problems.

Summarizing, we have presented the consequences of the microscopic spin-orbital model in the parameter regime relevant for cubic vanadates and suggested a scenario which explains the magnetic transition between the G -AF and dimerized C -AF phases observed in YVO_3 . This study indicates a close relationship between the observed magnetic correlations in the ground state and the

structural transition, which in case of YVO_3 occurs well above the first magnetic transition. Thus we conclude that a careful analysis of the mechanism of the structural transition and its dependence on the actual chemical composition is challenging and needed for complete theoretical understanding of the experimental phase diagram of cubic vanadates.

Acknowledgments

We thank B. Keimer and C. Ulrich for stimulating and insightful discussions. A. M. Oleś would like to acknowledge support by the Polish Ministry of Science and Education under Project No. N202 068 32/1481.

APPENDIX A: DERIVATION OF THE SPIN-ORBITAL MODEL

The effective superexchange interactions between two V^{3+} ions in d^2 configuration with spin $S = 1$ (triplet 3T_2 state) at sites i and j for a bond $\langle ij \rangle$ oriented along one of the cubic axes $\gamma = a, b, c$ originate from virtual charge excitations by the hopping processes which involve two active t_{2g} orbitals along its direction. As an example, we consider here a bond along c axis ($\gamma = c$), with active a (yz) and b (xz) orbitals. In this case the charge excitation by either a or b electron leads to one of three possible d^3 excited states: abc , a^2c or b^2c (see Fig. 2). The actual configuration c^1 of the inactive orbital c enters via the constraint (2.6). The total spin per two sites is conserved in the $d_i^2 d_j^2 \rightarrow d_i^3 d_j^1$ excitation process, i.e., the electron transferred in the excitation process and two other electrons on the d^3 site are either in high-spin ($S = \frac{3}{2}$) state, or in low-spin ($S = \frac{1}{2}$) state. Therefore, when the second order processes $d_i^2 d_j^2 \rightarrow d_i^3 d_j^1 \rightarrow d_i^2 d_j^2$ are analyzed, one has to project the d_i^3 configuration generated after an individual hopping process on the respective d_i^3 eigenstates. Similar, when a deexcitation process took place, one has to project the resulting d_i^2 configuration on the triplet 3T_2 ground state.

The general form of the effective Hamiltonian follows from symmetry considerations for the possible $d_i^2 d_j^2 \rightarrow d_i^3 d_j^1 \rightarrow d_i^2 d_j^2$ processes which contribute to the superexchange. The total spin states in the excited states are

well described by the spin operators:

$$\mathcal{P}_{\text{HS}}(\vec{S}_i, \vec{S}_j) = \frac{1}{S(2S+1)}(\vec{S}_i \cdot \vec{S}_j + 2), \quad (\text{A1})$$

$$\mathcal{P}_{\text{LS}}(\vec{S}_i, \vec{S}_j) = \frac{1}{S(2S+1)}(\vec{S}_i \cdot \vec{S}_j - 1), \quad (\text{A2})$$

which correspond to the high-spin $\mathcal{P}_{\text{HS}}(\vec{S}_i, \vec{S}_j)$ and low-spin $\mathcal{P}_{\text{LS}}(\vec{S}_i, \vec{S}_j)$ excited states, respectively. The orbital state is described by the orbital operators $\mathcal{Q}_n(i, j)$, where n refers to different excited states.¹⁰ In the present case $n = 1$ corresponds to high-spin $S = \frac{3}{2}$ excited states in Fig. 2(a), $n = 2$ to low-spin $S = \frac{1}{2}$ excited states in Fig. 2(b), while $n = 3$ describes the orbital state realized for the excitations of double occupancies shown in Fig. 2(c). As the orbital quantum number is conserved along the hopping process (2.2), either the same two orbitals are occupied before and after the virtual excitation, or an orbital fluctuation shown in Fig. 2 takes place, and the occupied orbitals are interchanged between sites i and j . The latter processes are unique for the t_{2g} orbitals and do not occur for degenerate and singly occupied e_g orbitals, where the orbital quantum number is not conserved and single orbital excitations are possible instead.¹⁵

In the case of cubic vanadates one arrives therefore at a general expression,

$$\begin{aligned} \mathcal{H} = \sum_{\langle ij \rangle} & \left\{ -\frac{1}{3} \frac{t^2}{\varepsilon(^4A_2)} (\vec{S}_i \cdot \vec{S}_j + 2) \mathcal{Q}_1(i, j) \right. \\ & + \frac{1}{3} \frac{t^2}{\varepsilon(^2E)} (\vec{S}_i \cdot \vec{S}_j - 1) \mathcal{Q}_2(i, j) \\ & \left. + \frac{1}{2} \left(\frac{t^2}{\varepsilon(^2T_1)} + \frac{t^2}{\varepsilon(^2T_2)} \right) (\vec{S}_i \cdot \vec{S}_j - 1) \mathcal{Q}_3(i, j) \right\}, \quad (\text{A3}) \end{aligned}$$

The first term $\propto t^2/\varepsilon(^4A_2)$ is FM, while the remaining terms stand for different AF contributions. The coefficient 1/2 in the contributions due to 2T_1 and 2T_2 excited states follows from the projection of the double occupancies of one of the active orbitals, either $a_i^2 c_i$ or $b_i^2 c_i$ [Fig. 2(c)], onto the eigenstates of V^{2+} ions. The orbital states which contribute to the above structure of superexchange (A3) depend on the bond direction; here we give as an example a complete expression for the bonds $\langle ij \rangle$ along the c -direction,

$$\begin{aligned}
\mathcal{H}_c = & \sum_{\langle ij \rangle \| c} \left\{ -\frac{1}{3} \frac{2t^2}{\varepsilon(4A_2)} (\vec{S}_i \cdot \vec{S}_j + 2) [(1 - n_{ia})(1 - n_{jb}) + (1 - n_{ib})(1 - n_{ja}) - (a_i^\dagger b_i b_j^\dagger a_j + b_i^\dagger a_i a_j^\dagger b_j) n_{ic} n_{jc}] \right. \\
& - \frac{1}{3} \frac{t^2}{\varepsilon(4A_2)} (\vec{S}_i \cdot \vec{S}_j + 2) [(1 - n_{ic}) n_{jc} + n_{ic} (1 - n_{jc})] \\
& + \frac{1}{3} \frac{2t^2}{\varepsilon(2E)} (\vec{S}_i \cdot \vec{S}_j - 1) [(1 - n_{ia})(1 - n_{jb}) + (1 - n_{ib})(1 - n_{ja}) + \frac{1}{2} (a_i^\dagger b_i b_j^\dagger a_j + b_i^\dagger a_i a_j^\dagger b_j) n_{ic} n_{jc}] \\
& + \frac{1}{3} \frac{t^2}{\varepsilon(2E)} (\vec{S}_i \cdot \vec{S}_j - 1) [(1 - n_{ic}) n_{jc} + n_{ic} (1 - n_{jc})] \\
& + \frac{1}{2} \left(\frac{t^2}{\varepsilon(2T_1)} + \frac{t^2}{\varepsilon(2T_2)} \right) (\vec{S}_i \cdot \vec{S}_j - 1) [(1 - n_{ia})(1 - n_{jb}) + (1 - n_{ib})(1 - n_{ja}) - n_{jc} - n_{ic} + 2] \\
& \left. + \frac{1}{2} \left(\frac{t^2}{\varepsilon(2T_1)} - \frac{t^2}{\varepsilon(2T_2)} \right) (\vec{S}_i \cdot \vec{S}_j - 1) \left(a_i^\dagger b_i a_j^\dagger b_j + b_i^\dagger a_i b_j^\dagger a_j \right) \right\}. \tag{A4}
\end{aligned}$$

The operators a_i^\dagger and b_i^\dagger are (spinless) fermion creation operators in the active orbitals $|a\rangle$ and $|b\rangle$ at site i , respectively, while $n_{i\gamma} = \gamma_i^\dagger \gamma_i$ are fermion number operators in state $|\gamma\rangle$ at site i , with $\gamma = a, b, c$.

The effective interactions on the bonds within the ab planes may be now obtained by rotating Eq. (A4) to the bonds oriented along either a or b axis. Note that the orbital operators which correspond to the active $|a\rangle$ and $|b\rangle$ orbitals are then replaced by either $|b\rangle$ and $|c\rangle$ (for a axis), or by $|a\rangle$ and $|c\rangle$ (for b axis), while the general structure of the superexchange Hamiltonian (A4) remains the same.

As both FM and AF terms are present in Eq. (A4), the superexchange interactions are frustrated. It is instructive to consider the limit of $J_H \rightarrow 0$ in which the multiplet structure of V^{2+} ions collapses to a single excitation energy U . In this case the interactions simplify considerably, and the terms $\propto n_{i\mu}$ which originate from the excitations with three different orbitals occupied at the same site cancel each other. This feature is analogous to the similar compensation of the high- and low-spin processes in the superexchange models with degenerate e_g orbitals.⁷ However, as a new feature one finds a nonvanishing contribution due to the orbital fluctuations, $\propto (a_i^\dagger b_i b_j^\dagger a_j + H.c.)$, as the terms which originate from the high- and low-spin processes add to each other. As usual, the double occupancies in the excited states lead to the AF terms as a consequence of the Pauli principle. These simplifications lead to the following form of the effective Hamiltonian along the c axis in the limit of $J_H \rightarrow 0$,

$$\begin{aligned}
\mathcal{H}_c(\eta = 0) = & J \sum_{\langle ij \rangle \| c} (\vec{S}_i \cdot \vec{S}_j + 1) \\
& \times \left(n_{ia} n_{jb} + n_{ib} n_{ja} + a_i^\dagger b_i b_j^\dagger a_j + b_i^\dagger a_i a_j^\dagger b_j \right), \tag{A5}
\end{aligned}$$

where $J = 4t^2/U$ is the superexchange interaction. This

expression may be also written in a more compact form,

$$\mathcal{H}_c(\eta = 0) = \frac{1}{2} J \sum_{\langle ij \rangle \| c} (\vec{S}_i \cdot \vec{S}_j + 1) \left(\vec{\tau}_i \cdot \vec{\tau}_j + \frac{1}{4} n_i n_j \right), \tag{A6}$$

where the scalar product of orbital pseudospin operators $\vec{\tau}_i = \{\tau_i^+, \tau_i^-, \tau_i^z\}$ is defined by:

$$\begin{aligned}
\tau_i^+ & \equiv a_i^\dagger b_i, & \tau_i^- & \equiv b_i^\dagger a_i, \\
\tau_i^z & \equiv \frac{1}{2} (n_{ia} - n_{ib}). \tag{A7}
\end{aligned}$$

Here we use spinless fermion operators a_i^\dagger and b_i^\dagger , but one could also introduce instead Schwinger boson operators. For the bonds along either a or b axis similar expressions obtained from Eqs. (A7) by cyclic permutations of the orbitals $\{a, b, c\}$ have to be used. If in addition the c orbitals are condensed ($n_{ic} = 1$), as in YVO_3 , one finds a simplified form of Eq. (A6) for the bonds along c axis,

$$\mathcal{H}_c^{(0)} = \frac{1}{2} J \sum_{\langle ij \rangle \| c} (\vec{S}_i \cdot \vec{S}_j + 1) \left(\vec{\tau}_i \cdot \vec{\tau}_j + \frac{1}{4} \right). \tag{A8}$$

The orbital interactions are then purely classical on the bonds in ab plane as $(\vec{\tau}_i \cdot \vec{\tau}_j + \frac{1}{4} n_i n_j)^{ab} \equiv \frac{1}{2}$ for these bonds.

APPENDIX B: SPIN AND ORBITAL EXCITATIONS IN THE DIMERIZED C -AF PHASE

Here we explain the full algebraic structure of the spin and orbital wave problem in the dimerized C -AF phase. Its solution gives the both types of excitation energies, and provides a systematic method to evaluate both the value of the order parameter,

$$\langle S_i^z \rangle \equiv S - \delta S^z, \tag{B1}$$

and the intersite spin correlations along c axis,

$$\langle \vec{S}_i \cdot \vec{S}_{i+1} \rangle \equiv \mathcal{C}_{i,i+1} = \mathcal{C}_0 + \delta\mathcal{C}e^{i\pi z_i}, \quad (\text{B2})$$

where z_i is the z th coordinate of the vector R_i corresponding to site i . If exchange interactions alternate along c axis, as given by Eqs. (5.7) and (5.8), the alternating part $\delta\mathcal{C}$ of the intersite spin correlation function is finite.

In order to evaluate the order parameter (B1) and the intersite spin correlations (B2) in the dimerized C -AF phase within the LSW formalism it is convenient to arrive first at the boson representation of the spin Hamiltonian. Therefore, we performed the transformation to a ferromagnet (4.9) and the subsequent Holstein-Primakoff transformation (4.10) to $\{a_i, a_i^\dagger\}$ bosons. One finds the following form of the above averages,

$$\delta S^z = S - \langle a_i^\dagger a_i \rangle, \quad (\text{B3})$$

$$\mathcal{C}_{i,i+1} = S^2 - 2\delta S^z + \langle a_i^\dagger a_{i+1}^\dagger \rangle, \quad (\text{B4})$$

and for the quadratic (LSW) Hamiltonian

$$\begin{aligned} H_{\text{LSW}} &= \mathcal{J}_{ab}^C \sum_{\langle ij \rangle \| ab} (n_i + n_j + a_i^\dagger a_j^\dagger + a_i a_j) \\ &+ \mathcal{J}_c^C \sum_{\langle i,i+1 \rangle \| c} \left(1 + e^{i\pi z_i} \delta_s \right) \\ &\times (n_i + n_{i+1} - a_{i+1}^\dagger a_i - a_i^\dagger a_{i+1}), \end{aligned} \quad (\text{B5})$$

where \mathcal{J}_c^C is the average value (5.10) of the FM exchange interaction along c axis.

Next we employ the Fourier transformation to boson operators in reciprocal (momentum) space

$$a_{\mathbf{k}}^\dagger = \frac{1}{\sqrt{N}} \sum_i e^{i\mathbf{k}\mathbf{R}_i} a_i^\dagger, \quad a_{\mathbf{k}} = \frac{1}{\sqrt{N}} \sum_i e^{-i\mathbf{k}\mathbf{R}_i} a_i, \quad (\text{B6})$$

which gives the LSW Hamiltonian in reciprocal space,

$$\begin{aligned} H_{\text{LSW}} &= \sum_{\mathbf{k}} \left\{ 4\mathcal{J}_{ab}^C a_{\mathbf{k}}^\dagger a_{\mathbf{k}} + 2\mathcal{J}_{ab}^C \gamma(\mathbf{k})(a_{\mathbf{k}}^\dagger a_{-\mathbf{k}}^\dagger + a_{-\mathbf{k}} a_{\mathbf{k}}) \right. \\ &\left. + 2\mathcal{J}_c^C [(1 - \cos k_z) a_{\mathbf{k}}^\dagger a_{\mathbf{k}} + i\delta_s \sin k_z a_{\mathbf{k}}^\dagger a_{\mathbf{k}+\mathbf{Q}}] \right\}, \end{aligned} \quad (\text{B7})$$

where $\mathbf{Q} = (0, 0, \pi)$ is the wave vector which corresponds to the doubling of the unit cell along c axis due to the dimerized C -AF spin structure.

In order to find both the energies of spin wave excitations and the average values of the correlation functions at finite temperature T , we introduce here temperature Green's functions for boson operators in the momentum space using the notation of Zubarev.^{65,66} The first of them satisfies the following equation of motion,

$$\omega \langle \langle a_{\mathbf{k}} | a_{\mathbf{k}}^\dagger \rangle \rangle_\omega = \frac{1}{2\pi} + \langle \langle [a_{\mathbf{k}}, H_{\text{LSW}}] | a_{\mathbf{k}}^\dagger \rangle \rangle_\omega. \quad (\text{B8})$$

It depends on energy ω and generates three more Green functions: $\langle \langle a_{\mathbf{k}+\mathbf{Q}} | a_{\mathbf{k}}^\dagger \rangle \rangle_\omega$, $\langle \langle a_{-\mathbf{k}} | a_{\mathbf{k}}^\dagger \rangle \rangle_\omega$, and $\langle \langle a_{-\mathbf{k}+\mathbf{Q}} | a_{\mathbf{k}}^\dagger \rangle \rangle_\omega$. It is next convenient to introduce the following expressions which define the algebraic structure of the spin wave problem:

$$A_{\mathbf{k}\pm} = 2\mathcal{J}_c^C (1 \pm \cos k_z) + 4\mathcal{J}_{ab}^C, \quad (\text{B9})$$

$$B_{\mathbf{k}} = 4\mathcal{J}_{ab}^C \gamma(\mathbf{k}), \quad (\text{B10})$$

$$\Delta_{\mathbf{k}} = 2\mathcal{J}_c^C \delta_s \sin k_z. \quad (\text{B11})$$

The respective system of equations of motion generated by Eq. (B8) is:

$$\begin{pmatrix} A_{\mathbf{k}-} - \omega_C(\mathbf{k}) & i\Delta_{\mathbf{k}} & B_{\mathbf{k}} & 0 \\ -i\Delta_{\mathbf{k}} & A_{\mathbf{k}+} - \omega_C(\mathbf{k}) & 0 & B_{\mathbf{k}} \\ -B_{\mathbf{k}} & 0 & -A_{\mathbf{k}-} - \omega_C(\mathbf{k}) & -i\Delta_{\mathbf{k}} \\ 0 & -B_{\mathbf{k}} & i\Delta_{\mathbf{k}} & -A_{\mathbf{k}+} - \omega_C(\mathbf{k}) \end{pmatrix} \begin{pmatrix} \langle \langle a_{\mathbf{k}} | a_{\mathbf{k}}^\dagger \rangle \rangle_\omega \\ \langle \langle a_{\mathbf{k}+\mathbf{Q}} | a_{\mathbf{k}}^\dagger \rangle \rangle_\omega \\ \langle \langle a_{-\mathbf{k}} | a_{\mathbf{k}}^\dagger \rangle \rangle_\omega \\ \langle \langle a_{-\mathbf{k}+\mathbf{Q}} | a_{\mathbf{k}}^\dagger \rangle \rangle_\omega \end{pmatrix} = -\frac{1}{2\pi} \begin{pmatrix} 1 \\ 0 \\ 0 \\ 0 \end{pmatrix}. \quad (\text{B12})$$

Eq. (B12) has a typical structure obtained for elementary excitations in the random phase approximation (or in the LSW theory) for an antiferromagnet. One finds two positive eigenvalues $\omega_{C\pm}(\mathbf{k})$ given by Eq. (5.12), and two negative ones, $-\omega_{C\pm}(\mathbf{k})$.

By solving the system of Eqs. (B8) one finds the following Green's functions:

$$\langle\langle a_{\mathbf{k}}|a_{\mathbf{k}}^\dagger \rangle\rangle_\omega = +\frac{1}{2\pi} \frac{(\omega^2 - A_{\mathbf{k}+}^2 + B_{\mathbf{k}}^2)(\omega + A_{\mathbf{k}-}) - \Delta_{\mathbf{k}}^2(\omega - A_{\mathbf{k}+})}{\{\omega^2 - \omega_{C+}^2(\mathbf{k})\}\{\omega^2 - \omega_{C-}^2(\mathbf{k})\}}, \quad (\text{B13})$$

$$\langle\langle a_{\mathbf{k}+\mathbf{Q}}|a_{\mathbf{k}}^\dagger \rangle\rangle_\omega = -\frac{i}{2\pi} \frac{\Delta_{\mathbf{k}}[(\omega + A_{\mathbf{k}+})(\omega + A_{\mathbf{k}-}) + B_{\mathbf{k}}^2 - \Delta_{\mathbf{k}}^2]}{\{\omega^2 - \omega_{C+}^2(\mathbf{k})\}\{\omega^2 - \omega_{C-}^2(\mathbf{k})\}}, \quad (\text{B14})$$

$$\langle\langle a_{-\mathbf{k}}^\dagger|a_{\mathbf{k}}^\dagger \rangle\rangle_\omega = -\frac{1}{2\pi} \frac{B_{\mathbf{k}}(\omega^2 - A_{\mathbf{k}+}^2 + B_{\mathbf{k}}^2 - \Delta_{\mathbf{k}}^2)}{\{\omega^2 - \omega_{C+}^2(\mathbf{k})\}\{\omega^2 - \omega_{C-}^2(\mathbf{k})\}}, \quad (\text{B15})$$

$$\langle\langle a_{-\mathbf{k}+\mathbf{Q}}^\dagger|a_{\mathbf{k}}^\dagger \rangle\rangle_\omega = +\frac{i}{2\pi} \frac{\Delta_{\mathbf{k}}B_{\mathbf{k}}(A_{\mathbf{k}+} + A_{\mathbf{k}-})}{\{\omega^2 - \omega_{C+}^2(\mathbf{k})\}\{\omega^2 - \omega_{C-}^2(\mathbf{k})\}}. \quad (\text{B16})$$

They contain complete information about the bosonic correlation functions which appear in Eqs. (B3) and (B4). They are obtained from the temperature Green's functions using the fluctuation-dissipation theorem,⁶⁵

$$\begin{aligned} \delta S^z &= \frac{1}{N} \sum_{\mathbf{k}} \langle a_{\mathbf{k}}^\dagger a_{\mathbf{k}} \rangle \\ &= \frac{1}{N} \sum_{\mathbf{k}} \int d\omega \frac{2\Im \langle\langle a_{\mathbf{k}}|a_{\mathbf{k}}^\dagger \rangle\rangle_{\omega-i\epsilon}}{e^{\beta\omega} - 1}, \end{aligned} \quad (\text{B17})$$

$$\begin{aligned} \delta \mathcal{C} &= \frac{1}{N} \sum_{\mathbf{k}} \langle a_{\mathbf{k}}^\dagger a_{\mathbf{k}+\mathbf{Q}} \rangle \\ &= \frac{1}{N} \sum_{\mathbf{k}} \int d\omega \frac{2\Im \langle\langle a_{-\mathbf{k}}^\dagger|a_{\mathbf{k}}^\dagger \rangle\rangle_{\omega-i\epsilon}}{e^{\beta\omega} - 1}, \end{aligned} \quad (\text{B18})$$

where $\beta = 1/k_B T$.

In a similar way one may find the orbital excitations and the respective Green's functions needed to determine the alternation of the orbital correlations in the dimerized structure,

$$\langle \vec{\tau}_i \cdot \vec{\tau}_{i+1} \rangle \equiv \mathcal{T}_{i,i+1} = \mathcal{T}_{i,i+1}^{(0)} + \delta \mathcal{T} e^{i\pi z_i}, \quad (\text{B19})$$

and the renormalized value of the order parameter,

$$\langle \tau_i^z \rangle \equiv \frac{1}{2} - \delta \tau^z. \quad (\text{B20})$$

As in case of spin operators, we used the rotation (4.16) of orbital operators to the ferro orbital state, followed by the Holstein-Primakoff transformation (4.17) to the respective boson operators $\{b_i, b_i^\dagger\}$. One finds the LOW Hamiltonian,

$$\begin{aligned} H_{\text{LOW}} &= J\eta(r_1 + r_3) \sum_{\langle ij \rangle \| ab} (p_i + p_j) \\ &+ J \sum_{\langle i,i+1 \rangle \| c} \left\{ \left[R - \frac{1}{2} \mathcal{C}_0 [r_1 - \eta(r_1 + r_3)] \right] (p_i + p_{i+1}) \right. \\ &+ \left. \left[R - \frac{1}{2} \mathcal{C}_0 [r_1 - \eta r_1 (1 - \eta)] \right] (b_{i+1}^\dagger b_i + b_i^\dagger b_{i+1}) \right\} \\ &+ \frac{1}{2} J \mathcal{C}_0 \delta_o r_1 (1 - \eta) \sum_{\langle i,i+1 \rangle \| c} (b_{i+1}^\dagger b_i + b_i^\dagger b_{i+1}). \end{aligned} \quad (\text{B21})$$

where $p_i = b_i^\dagger b_i$.

In spite of the 1D nature of orbital dispersion (4.18), the Fourier transformation to boson operators in the reciprocal (momentum) space is three-dimensional and takes here the form

$$b_{\mathbf{k}}^\dagger = \frac{1}{\sqrt{N}} \sum_i e^{ik_z z_i} b_i^\dagger, \quad b_{\mathbf{k}} = \frac{1}{\sqrt{N}} \sum_i e^{-ik_z z_i} b_i, \quad (\text{B22})$$

Similar to spin case, we find the energies of orbital wave excitations and the average values of the boson operators at finite temperature T , using temperature Green's functions for boson operators in momentum space.^{65,66} The system of equations is generated by the following equation of motion,

$$\omega \langle\langle b_{\mathbf{k}}|b_{\mathbf{k}}^\dagger \rangle\rangle_\omega = \frac{1}{2\pi} + \langle\langle [b_{\mathbf{k}}, H_{\text{LOW}}] | b_{\mathbf{k}}^\dagger \rangle\rangle_\omega, \quad (\text{B23})$$

and equations for three other Green functions: $\langle\langle b_{\mathbf{k}+\mathbf{Q}}|b_{\mathbf{k}}^\dagger \rangle\rangle_\omega$, $\langle\langle b_{-\mathbf{k}}|b_{\mathbf{k}}^\dagger \rangle\rangle_\omega$, and $\langle\langle b_{-\mathbf{k}+\mathbf{Q}}|b_{\mathbf{k}}^\dagger \rangle\rangle_\omega$, follow. The following expressions define the algebraic structure of the orbital problem:

$$\begin{aligned} \bar{A}_{\mathbf{k}} &= r_1 + \eta(r_1 + r_3) - \frac{1}{2}(1 - \mathcal{C}_0)[r_1 - \eta(r_1 + r_3)] \\ &+ \frac{1}{2}(1 + 2\eta r_1 - \eta r_3) Y_{ab}, \end{aligned} \quad (\text{B24})$$

$$\bar{B}_{\mathbf{k}} = \left[r_1 - \frac{1}{2}(1 - \mathcal{C}_0)r_1(1 - \eta) \right], \quad (\text{B25})$$

$$\Theta_{\mathbf{k}} = \frac{1}{2}(1 - \mathcal{C}_0)\delta_o r_1(1 - \eta) \sin k_z. \quad (\text{B26})$$

Here we used the short hand notation for the spin correlation function in ab planes,

$$Y_{ab} \equiv \langle \vec{S}_i \cdot \vec{S}_j \rangle + 1, \quad (\text{B27})$$

for a bond $\langle ij \rangle \| ab$.

The respective system of equations of motion has a similar structure to that of Eq. (B8) is:

$$\begin{pmatrix} \bar{A}_{\mathbf{k}} - \Omega_C(\mathbf{k}) & i\Theta_{\mathbf{k}} & \bar{B}_{\mathbf{k}} & 0 \\ -i\Theta_{\mathbf{k}} & \bar{A}_{\mathbf{k}} - \Omega_C(\mathbf{k}) & 0 & -\bar{B}_{\mathbf{k}} \\ -\bar{B}_{\mathbf{k}} & 0 & -\bar{A}_{\mathbf{k}} - \Omega_C(\mathbf{k}) & -i\Theta_{\mathbf{k}} \\ 0 & \bar{B}_{\mathbf{k}} & i\Theta_{\mathbf{k}} & -\bar{A}_{\mathbf{k}} - \Omega_C(\mathbf{k}) \end{pmatrix} \begin{pmatrix} \langle\langle b_{\mathbf{k}}|b_{\mathbf{k}}^\dagger \rangle\rangle_\omega \\ \langle\langle b_{\mathbf{k}+\mathbf{Q}}|b_{\mathbf{k}}^\dagger \rangle\rangle_\omega \\ \langle\langle b_{-\mathbf{k}}^\dagger|b_{\mathbf{k}}^\dagger \rangle\rangle_\omega \\ \langle\langle b_{-\mathbf{k}+\mathbf{Q}}^\dagger|b_{\mathbf{k}}^\dagger \rangle\rangle_\omega \end{pmatrix} = -\frac{1}{2\pi} \begin{pmatrix} 1 \\ 0 \\ 0 \\ 0 \end{pmatrix}. \quad (\text{B28})$$

The Green functions can be now found from Eqs. (B28). They contain complete information about the bosonic correlation functions which appear in Eqs. (B19) and (B20). They are obtained from the temperature Green's functions using the fluctuation-dissipation theorem,⁶⁵

$$\begin{aligned} \delta\tau^z &= \frac{1}{N} \sum_{\mathbf{k}} \langle b_{\mathbf{k}}^\dagger b_{\mathbf{k}} \rangle \\ &= \frac{1}{N} \sum_{\mathbf{k}} \int d\omega \frac{2\Im \langle\langle b_{\mathbf{k}}|b_{\mathbf{k}}^\dagger \rangle\rangle_{\omega-i\epsilon}}{e^{\beta\omega} - 1}, \end{aligned} \quad (\text{B29})$$

$$\begin{aligned} \delta\mathcal{T} &= \frac{1}{N} \sum_{\mathbf{k}} \langle b_{\mathbf{k}}^\dagger b_{\mathbf{k}+\mathbf{Q}} \rangle \\ &= \frac{1}{N} \sum_{\mathbf{k}} \int d\omega \frac{2\Im \langle\langle b_{-\mathbf{k}}^\dagger|b_{\mathbf{k}}^\dagger \rangle\rangle_{\omega-i\epsilon}}{e^{\beta\omega} - 1}. \end{aligned} \quad (\text{B30})$$

The values of the orbital correlation functions Eqs. (B19) and (B20) in the dimerized structure were used together with the respective spin correlation functions Eqs. (B3) and (B3) to obtain the self-consistent solution of Fig. 13.

-
- ¹ M. Imada, A. Fujimori, and Y. Tokura, *Rev. Mod. Phys.* **70**, 1039 (1998).
- ² S. Maekawa, T. Tohyama, S. E. Barnes, S. Ishihara, W. Koshibae, and G. Khaliullin, *Physics of Transition Metal Oxides*, Springer Series in Solid State Sciences Vol. 144 (Springer-Verlag, Heidelberg, 2004).
- ³ J. Zaanen and A. M. Oleś, *Phys. Rev. B* **48**, 7197 (1993).
- ⁴ K. I. Kugel and D. I. Khomskii, *Usp. Fiz. Nauk* **136**, 621 (1982) [*Sov. Phys. Usp.* **25**, 231 (1982)].
- ⁵ J. B. Goodenough, *Magnetism and Chemical Bond* (Interscience, New York, 1963).
- ⁶ Y. Tokura and N. Nagaosa, *Science* **288**, 462 (2000).
- ⁷ A. M. Oleś, *Phys. Stat. Sol. (b)* **236**, 281 (2003); (E) **242**, 963 (2005).
- ⁸ G. Khaliullin, *Prog. Theor. Phys. Suppl.* **160**, 155 (2005).
- ⁹ A. M. Oleś, G. Khaliullin, P. Horsch, and L. F. Feiner, *Phys. Rev. B* **72**, 214431 (2005).
- ¹⁰ G. Khaliullin, P. Horsch, and A. M. Oleś, *Phys. Rev. B* **70**, 195103 (2004).
- ¹¹ L. F. Feiner, A. M. Oleś, and J. Zaanen, *Phys. Rev. Lett.* **78**, 2799 (1997).
- ¹² G. Khaliullin and V. Oudovenko, *Phys. Rev. B* **56**, R14 243 (1997); G. Khaliullin and R. Kilian, *J. Phys.: Condens. Matter* **11**, 9757 (1999).
- ¹³ L. F. Feiner and A. M. Oleś, *Phys. Rev. B* **59**, 3295 (1999).
- ¹⁴ S. Okamoto, S. Ishihara, and S. Maekawa, *Phys. Rev. B* **65**, 144403 (2002).
- ¹⁵ L. F. Feiner, A. M. Oleś, and J. Zaanen, *J. Phys.: Condens. Matter* **10**, L555 (1998); A. M. Oleś, L. F. Feiner, and J. Zaanen, *Phys. Rev. B* **61**, 6257 (2000).
- ¹⁶ K. I. Kugel and D. I. Khomskii, *Sov. Phys. JETP* **37**, 725 (1973).
- ¹⁷ M. Cyrot and C. Lyon-Caen, *J. Phys. (Paris)* **36**, 253 (1975); S. Inagaki, *J. Phys. Soc. Jpn.* **39**, 596 (1975).
- ¹⁸ C. Castellani, C. R. Natoli, and J. Ranninger, *Phys. Rev. B* **18**, 4945 (1978); **18**, 4967 (1978); **18**, 5001 (1978).
- ¹⁹ G. Khaliullin and S. Maekawa, *Phys. Rev. Lett.* **85**, 3950 (2000); G. Khaliullin, *Phys. Rev. B* **64**, 212405 (2001).
- ²⁰ B. Keimer, D. Casa, A. Ivanov, J. W. Lynn, M. v. Zimmermann, J. P. Hill, D. Gibbs, Y. Taguchi, and Y. Tokura, *Phys. Rev. Lett.* **85**, 3946 (2000).
- ²¹ A. M. Oleś, P. Horsch, L. F. Feiner, and G. Khaliullin, *Phys. Rev. Lett.* **96**, 147205 (2006).
- ²² W. Bao, C. Broholm, G. Aeppli, P. Dai, J. M. Honig, and P. Metcalf, *Phys. Rev. Lett.* **78**, 507 (1997).
- ²³ T. Mizokawa and A. Fujimori, *Phys. Rev. B* **54**, 5368 (1996).
- ²⁴ S. Di Matteo, N. B. Perkins, and C. R. Natoli, *Phys. Rev. B* **65**, 054413 (2002).
- ²⁵ A. V. Mahajan, D. C. Johnston, D. R. Torgenson, and F. Borsa, *Phys. Rev. B* **46**, 10 966 (1992).
- ²⁶ H. C. Nguyen and J. B. Goodenough, *Phys. Rev. B* **52**, 324 (1995).
- ²⁷ S. Miyasaka, T. Okuda, and Y. Tokura, *Phys. Rev. Lett.* **85**, 5388 (2000).
- ²⁸ Y. Ren, A. A. Nugroho, A. A. Menovsky, J. Strempler, U. Rütt, F. Iga, T. Takabatake, and C. W. Kimball, *Phys. Rev. B* **67**, 014107 (2003).
- ²⁹ S. Miyasaka, Y. Okimoto, M. Iwama, and Y. Tokura, *Phys. Rev. B* **68**, 100406(R) (2003); J. Fujioka, S. Miyasaka, and Y. Tokura, *Phys. Rev. B* **72**, 024460 (2005).
- ³⁰ S. Miyasaka, J. Fujioka, M. Iwama, Y. Okimoto, and Y. Tokura, *Phys. Rev. B* **73**, 224436 (2006).
- ³¹ M. Raczkowski and A. M. Oleś, *Phys. Rev. B* **66**, 094431

- (2002).
- ³² H. Kawano, H. Yoshizawa, and Y. Ueda, *J. Phys. Soc. Jpn.* **63**, 2857 (1994).
- ³³ Y. Ren, T. T. M. Palstra, D. I. Khomskii, A. A. Nugroho, A. A. Menovsky, and G. A. Sawatzky, *Phys. Rev. B* **62**, 6577 (2000); M. Noguchi, A. Nakazawa, S. Oka, T. Arima, Y. Wakabayashi, H. Nakao, and Y. Murakami, *ibid.* **62**, R9271 (2000).
- ³⁴ G. R. Blake, T. T. M. Palstra, Y. Ren, A. A. Nugroho, and A. A. Menovsky, *Phys. Rev. Lett.* **87**, 245501 (2001); *Phys. Rev. B* **65**, 174112 (2002).
- ³⁵ M. Reehuis, C. Ulrich, P. Pattison, B. Ouladdiaf, M. C. Rheinstädter, M. Ohl, L. P. Regnault, M. Miyasaka, Y. Tokura, and B. Keimer, *Phys. Rev. B* **73**, 094440 (2006).
- ³⁶ C. Ulrich, G. Khaliullin, J. Sirker, M. Reehuis, M. Ohl, S. Miyasaka, Y. Tokura, and B. Keimer, *Phys. Rev. Lett.* **91**, 257202 (2003).
- ³⁷ P. Horsch, G. Khaliullin, and A. M. Oleś, *Phys. Rev. Lett.* **91**, 257203 (2003).
- ³⁸ H. Sawada, N. Hamada, K. Terakura, and T. Asada, *Phys. Rev. B* **53**, 12742 (1996); H. Sawada and K. Terakura, *ibid.* **58**, 6831 (1998).
- ³⁹ I. V. Solovyev, *Phys. Rev. B* **74**, 054412 (2006).
- ⁴⁰ V. I. Anisimov, J. Zaanen, and O. K. Andersen, *Phys. Rev. B* **44**, 943 (1991).
- ⁴¹ T. Mizokawa, D. I. Khomskii, and G. A. Sawatzky, *Phys. Rev. B* **60**, 7309 (1999).
- ⁴² G. Khaliullin, P. Horsch, and A. M. Oleś, *Phys. Rev. Lett.* **86**, 3879 (2001).
- ⁴³ M. Cuoco, F. Forte, and C. Noce, *Phys. Rev. B* **74**, 195124 (2006).
- ⁴⁴ A. M. Oleś, *Phys. Rev. B* **28**, 327 (1983).
- ⁴⁵ J. Kanamori, *J. Appl. Phys.* **31**, 14S (1960).
- ⁴⁶ J. S. Griffith, *The Theory of Transition Metal Ions* (Cambridge University Press, Cambridge, 1971).
- ⁴⁷ J. Zaanen and G. A. Sawatzky, *J. Solid State Chem.* **88**, 8 (1990).
- ⁴⁸ The excitation energies to $t_{2g}^3 t_{2g}^1$ configuration on a bond $\langle ij \rangle$ expressed in terms of the Racah parameters are: $A - 5B$ (4A_2), $A + 4B + 3C$ (2E and 2T_1), and $A + 10B + 5C$ (2T_2); this spectrum is rigorously reproduced with U and J_H given by Eqs. (2.5), see Ref. 46.
- ⁴⁹ The off-diagonal elements of the Coulomb interaction $\propto J_H$ are also responsible for the propagation of longitudinal orbital excitations in e_g systems, as explained in Ref. 15.
- ⁵⁰ This is in contrast to the $S = 1/2$ case, where (spin-singlet) \times (orbital-triplet) and (spin-triplet) \times (orbital-singlet) configurations are *degenerate*, resulting in a strong quantum resonance between them, as discussed in Ref. 19.
- ⁵¹ M. Kohmoto, *Phys. Rev. B* **37**, 3812 (1988); S.-Q. Shen, *ibid.* **64**, 132411 (2001).
- ⁵² A. M. Oleś, G. Khaliullin, and P. Horsch, *Acta Phys. Polon. B* **34**, 857 (2003).
- ⁵³ S. Q. Shen, X. C. Xie, and F. C. Zhang, *Phys. Rev. Lett.* **88**, 027201 (2002).
- ⁵⁴ J. Kanamori, *J. Phys. Chem. Solids* **10**, 87 (1959).
- ⁵⁵ C. Mattis, *The Theory of Magnetism I*, (Springer, Berlin, 1981).
- ⁵⁶ M. Takahashi, *Phys. Rev. B* **40**, 2494 (1989).
- ⁵⁷ J. Sirker and G. Khaliullin, *Phys. Rev. B* **67**, 100408(R) (2003); S. Miyashita, A. Kawaguchi, N. Kawakami, and G. Khaliullin, *ibid.* **69**, 104425 (2004).
- ⁵⁸ S. Miyasaka, S. Onoda, Y. Okimoto, J. Fujioka, M. Iwama, N. Nagaosa, and Y. Tokura, *Phys. Rev. Lett.* **94**, 076405 (2005).
- ⁵⁹ J. van der Brink, P. Horsch, F. Mack, and A. M. Oleś, *Phys. Rev. B* **59**, 6795 (1999).
- ⁶⁰ S. Ishihara, *Phys. Rev. B* **69**, 075118 (2004).
- ⁶¹ This correction could easily be included but it does not modify the qualitative conclusions — this energy contribution would only slightly modify the critical value of V in the phase diagram of Fig. 8.
- ⁶² P. Jordan and E. Wigner, *Z. Phys.* **47**, 631 (1928).
- ⁶³ S. Ishihara and S. Maekawa, *Phys. Rev. B* **62**, 2338 (2000); S. Okamoto, S. Ishihara, and S. Maekawa, *ibid.* **66**, 014435 (2002).
- ⁶⁴ C. Ulrich, A. Gössling, M. Grüninger, M. Guennou, H. Roth, M. Cwik, T. Lorenz, G. Khaliullin, and B. Keimer, *Phys. Rev. Lett.* **97**, 157401 (2006).
- ⁶⁵ D. N. Zubarev, *Sov. Usp. Phys.* **3**, 320 (1960).
- ⁶⁶ S. B. Haley and P. Erdős, *Phys. Rev. B* **5**, 1106 (1972).